
**TRIBHUVAN UNIVERSITY**
**INSTITUTE OF ENGINEERING**
**PULCHOWK CAMPUS**

# DESIGN, FABRICATION, AND CHARACTERIZATION OF PISTON DRIVEN SUPERSONIC SHOCK TUBE

**By:**
**Bhawana Pokharel (077BAS004)**
**Jaya Paudel (077BAS015)**
**Prajit Dhakal (077BAS029)**
**Prashant Sharma Prasar (077BAS030)**

**SUBMITTED TO THE DEPARTMENT OF MECHANICAL AND AEROSPACE ENGINEERING IN PARTIAL FULFILLMENT OF THE REQUIREMENT FOR THE DEGREE OF BACHELOR IN AEROSPACE ENGINEERING**

**DEPARTMENT OF MECHANICAL AND AEROSPACE ENGINEERING**
**LALITPUR, NEPAL**

**April, 2025**

# COPYRIGHT

# TRIBHUVAN UNIVERSITY
# INSTITUTE OF ENGINEERING
# PULCHOWK CAMPUS
# DEPARTMENT OF MECHANICAL AND AEROSPACE ENGINEERING

## LETTER OF APPROVAL

The undersigned certify that they have read, and recommended to the Institute of Engineering for acceptance, a project report entitled ***"Design, Fabrication and Characterization of Piston Driven Supersonic Shock Tube"*** submitted by **Bhawana Pokharel, Jaya Paudel, Prajit Dhakal, Prashant Sharma Prasar** in partial fulfillment of the requirements for the Bachelor's Degree in Aerospace Engineering.

---

**Supervisor: Sudip Bhattrai (PhD)**
Assistant Professor
Department of Mechanical and Aerospace Engineering
Institute of Engineering, Pulchowk Campus

---

**External Examiner: Er. Akin Chhetri**
MEP Engineer
Kathmandu Iternational Hospital.

---

**Head of Department: Sudip Bhattrai (PhD)**
Assistant Professor
Department of Mechanical and Aerospace Engineering
Institute of Engineering, Pulchowk Campus

**Date of Approval:** 10th March, 2025

## ABSTRACT

A shock tube is a device used to generate and study high-speed shock waves and the phenomena associated with them. This study presents the design, fabrication and characterization of a piston-driven shock tube, a compact and low-cost device designed to produce supersonic flow. The study uses a high-frequency Data Acquisition(DAQ) system comprised of NI X Series USB 6341. The electronics system measures pressure voltage from the transducer, amplifies it, and sends the output to the DAQ system for visualization in LabVIEW. The study utilizes ToF method with a 100 mm transducer spacing for the velocity measurement. A maximum shockwave mach number upto 1.723 was achieved using 0.072mm aluminum diaphragm at maximum burst pressure ratio of 14.239, characterized by x/l ratio. Schlieren imaging is used to visualize the shockwave and flow patterns behind it.



***Keywords****: piston-driven shock tube, Shock-wave,Pressure Transducer, DAQ, LabVIEW, ToF, supersonic*

## ACKNOWLEDGEMENT

Foremost, we would like to express our sincere appreciation to **Dr.Sudip Bhattrai**, our project supervisor, for his constant guidance, inspiring lectures and encouragement. His valuable insights on this project and beyond have been immensely instrumental to us. We sincerely acknowledge his supervision and expertise.

We extend our gratitude to the **Department of Mechanical and Aerospace Engineering**, Institute of Engineering, Pulchowk Campus, for providing us opportunity to engage in collaborative project. This experience has allowed us to apply the knowledge acquired throughout the four years to our final year major project. Furthermore, it has allowed us to undertake our own project, strengthening our ability to apply theoretical concepts to practical applications.

We sincerely appreciate the guidance and support of **Mr. Akin Chhetri**, MSMDE 2078 senior from IOE Pulchowk. His MSc. thesis, "Development and Experimental Verification of a Manual Piston-Driven Hypersonic Shock Tunnel," has been a valuable source of inspiration for our work.

We would like to thank **Mr. Salim Maharjan** for his assistance in obtaining the Schlieren images for our project. His expertise in optical instruments and the flow visualization technique has been invaluable in our project. Additionally, we extend our gratitude to the Flow Visualization Laboratory of Mechanical and Aerospace Engineering for providing us with the required instruments for flow visualization.

We also extend our thanks to all of our friends, seniors and juniors, especially our senior, MSMDE student, **Mr Chandrika Nanda Adhikari** for their direct and indirect support for the project. Last but not the least, we give a deep sense of appreciation to our family members who have been a constant source of inspiration for us.

Any kind of suggestion or criticism that may contribute to the progress of our project will be greatly appreciated and acknowledged.

**Authors:**
Bhawana Pokharel
Jaya Paudel
Prajit Dhakal
Prashant Sharma Prasar

## CONTENTS

## LIST OF TABLES

## LIST OF FIGURES

## LIST OF ABBREVIATIONS

| | |
|---|---|
| **2D** | Two Dimensional |
| **3D** | Three Dimensional |
| **AI** | Analog Input |
| **CAD** | Computer Aided Drawing |
| **C-D** | Converging Diverging |
| **CFD** | Computational Fluid Dynamics |
| **DAQ** | Data Acquisition |
| **DC** | Direct Current |
| **DMAE** | Department of Mechanical and Aerospace Engineering |
| **FPS** | Frames Per Second |
| **FSO** | Full Scale Output |
| **GCI** | Grid Convergence Index |
| **GND** | Ground |
| **GSM** | Grams per Square Meter |
| **HST** | Hypersonic Shock Tunnel |
| **IISc** | Indian Institute of Science |
| **I/O** | Input/Output |
| **LabVIEW** | Laboratory Virtual Instrument Engineering Workbench |
| **MEMS** | Micro Electro Mechanical Sensor |
| **MS** | Mild Steel |
| **NI** | National Instruments |
| **PLA** | Polylactic Acid |
| **PCB** | Printed Circuit Board |
| **ppm** | Parts per Million |
| **SS** | Stainless Steel |
| **tdms** | Technical Data Management System |
| **ToA** | Time of Arrival |
| **ToF** | Time of Flight |
| **USB** | Universal Serial Bus |
| **VI** | Virtual Instrument |

## LIST OF SYMBOLS

| | |
|---|---|
| $\mu$s | Microsecond |
| $\gamma$ | Specific Heat Ratio |
| $C$ | Celsius |
| $R$ | Gas Constant |
| $\rho$ | Density of air |
| $M$ | Mach Number |
| $M_s$ | Shock Mach Number |
| $a$ | Speed of sound |
| $mm$ | Millimeter |
| $P_1$ | Pressure before shock |
| $P_4$ | Pressure after shock |
| $T$ | Temperature |
| $\Delta$x | Distance between two transducer |
| $Pa$ | Pascal |
| $f$ | Focal length |
| $u$ | Velocity |
| $V$ | Volume |
| $l$ | Length of Driver Section |
| $atm$ | Standard Atmospheric Pressure |
| $S$ | Shock Waves |
| $E$ | Expansion Waves |
| $mV$ | Millivolts |
| $R_{comp}$ | Compensating Resistance |
| $Ks$ | Kilo samples |
| ms | Millisecond |

# CHAPTER ONE:
# INTRODUCTION

## 1.1 Background

A normal shock wave is a discontinuity that forms perpendicular to the upstream flow, resulting in abrupt changes in pressure, temperature, and velocity. A normal shock wave can be observed in front of a blunt body, within a supersonic nozzle, in explosion waves from gas dynamics, as well as in shock tubes, Ludwieg tubes, and various other applications. In the case of a blunt body, the normal portion of a bow shock wave forms ahead of the object, and the streamline passing through this region later impinges on the nose. This interaction plays a critical role in determining the stagnation (total) pressure and temperature at the nose, making the flow properties behind the shock wave highly significant for aerodynamic performance and heat transfer analysis. Supersonic flow is established inside a nozzle, where the back pressure is high enough to cause a normal shock wave to stand inside the nozzle.

A shock wave can either remain stationary or propagate, depending on the flow conditions. When a shock wave moves into an opposing supersonic flow at the same velocity, the wave appears stationary, forming a standing normal shock wave. This balance results in a steady flow with supersonic conditions upstream and subsonic conditions downstream of the shock. However, if the opposing flow is removed, the shock wave propagates freely, inducing mass motion behind it and transitioning the system from a steady to an unsteady state. This transition is particularly relevant in applications such as shock tubes, where moving shock waves generate rapid pressure and temperature changes that drive unsteady flow dynamics.

A shock tube is a laboratory tool that can create varying flow speeds and regimes, commonly used for investigating shock waves. These waves result from the sudden release of energy, high-speed projectiles, and laser ablations. Shock waves are a common occurrence in daily life and it has applications in diverse fields, like aerodynamics, biomedical science, chemical kinetics, and industrial processes. A conventional cylindrical shock tube consists of two sections separated by a diaphragm, the driver section, and the driven section, respectively. Each section contains gas initially held at different pressures, and the type could be the same or different in both sections. The driver section contains gas held at a higher pressure than the driven section. Placing instrumentation on the long side or the end of the driven section, measurements of pressures can be done.

The release of pressure at the diaphragm causes an expansion wave to propagate back into the driver section. Simultaneously, a contact surface between the driver and driven gases, which moves more slowly than the shock wave, propagates along the tube behind the shock front. The length of the driven tube section and the relative velocity between the shock wave and contact surface ultimately determine the time over which useful measurements can be made.

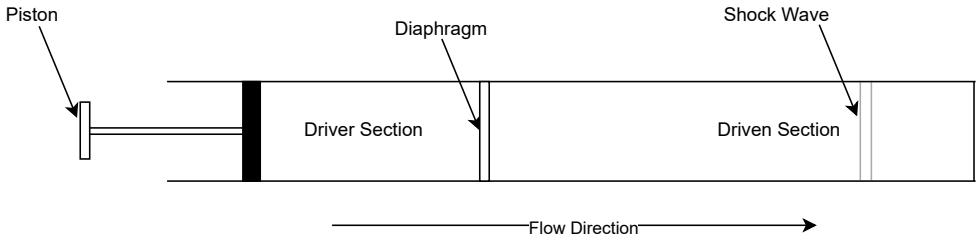


Figure 1.1: Piston-driven Shock Tube

## 1.2 Shock Tube

The simplest model of a shock tube consists of creating a moving shock wave in a tube of constant (circular or rectangular) cross-section, which generates a flow at high temperature and out of equilibrium. Ideally, this flow is one-dimensional and non-dissipating.

Schematically, a tube initially containing the test gas (low-pressure chamber) is separated by a diaphragm from another chamber (high-pressure chamber or driver section) containing another gas (driver gas). After the rupture of this diaphragm, the driver gas expands into the low-pressure chamber and generates a shock wave which propagates into the driven section. The shock wave gives the test gas a brutal acceleration, accompanied by a jump in temperature, pressure, and density. Physical and chemical processes can then start and possibly evolve to their equilibrium state. The test gas flow is limited by a contact surface (or interface) separating this flow from the driver gas flow and, in current installations of a few meters in length, this flow generally lasts a few hundred microseconds. In the assumed absence of dissipative phenomena, the shock wave preserves a constant speed and, therefore, in a reference frame fixed to this shock wave, the flow is one-dimensional and stationary. Moreover, if the rupture of the diaphragm is assumed instantaneous, a system of centered rarefaction waves develops in the expanding driver gas. In addition, the pressure and velocity are preserved through the interface, whereas the temperature and the density undergo a discontinuity.

## 1.3 Reflected Shock wave

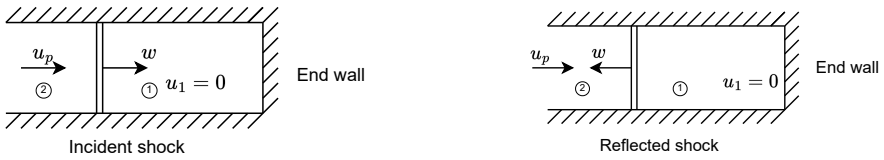


(a) Incident Shock waves

(b) Reflected shock waves

Figure 1.2: Normal shock wave propagation upon reflection

At the end of a closed tube, the shock wave is reflected back into the gas which is already compressed and heated by the incident shock wave. Upon reflection of the shock wave,

a new uniform state is formed where the particle velocity behind the reflected shock is zero, but extremely high temperatures, densities, and pressures are attained. After normal reflection the shock wave eventually refracts at the contact front produced by the ruptured diaphragm. When the rarefaction wave reflects from the chamber wall, it also forms a new uniform state of extremely low temperatures, densities and pressures, and zero particle velocity. The rarefaction wave generated by the ruptured diaphragm undergoes normal reflection at the end of the chamber and refracts at the contact surface. It is theoretically possible to achieve a total vacuum in this state[1].

## 1.4 Pressure distribution across a shock-wave

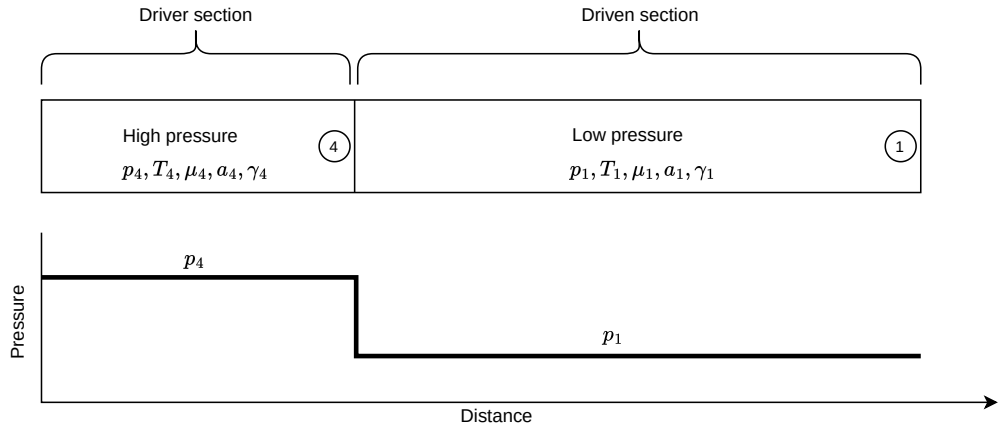


Figure 1.3: Initial condition in a pressure-driven shock tube

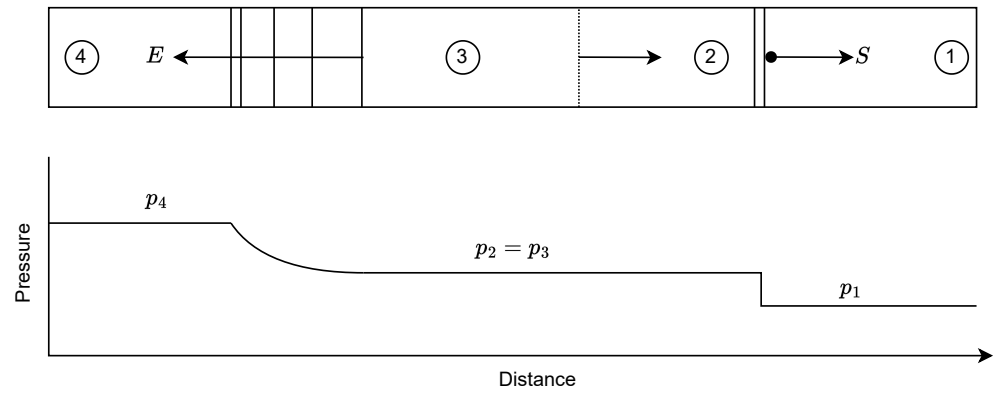


Figure 1.4: Flow in a shock tube after diaphragm is burst

As shown in the above figures, section (4), which is the driver section, is compressed to a higher pressure ($P_4$). Section (1), which is the driven section, is at ambient pressure($P_1$). Since the diaphragm is placed between the two sections and acts as a barrier for pressure interaction, there is a sharp decrease in pressure across it. This pressure distribution is presented in the plot above the initial condition of the shock tube before rupturing the

diaphragm, as shown in Fig. 1.3.

After the diaphragm is ruptured, a normal shock wave $(S)$ propagates into the driven section (1), acting as a piston and giving a sudden rise in pressure and temperature. Due to the falling pressure in the driver section, an expansion wave (E) is generated that propagates into section (4) with a gradual decrease in pressure and temperature. This creates an instantaneous section (2) and (3) between the expansion wave and normal shock wave. Here, section (2) is the part of the driven gas that is raised in pressure and temperature after the normal shock, and section (3) is the part where the driver gas propagates after the diaphragm burst. This creates an equilibrium in the (2) and (3) sections with a surface of interaction between them. The propagation of the shocks after the rupturing of the diaphragm and the pressure distribution at that instant are shown in Fig. 1.4. The purpose is to create a shock wave by the breaking of the diaphragm. The downstream of the shock wave has low pressure whereas the upstream of the shock wave has high pressure. The ratio of these pressures is a function of the Mach number [2].

$$\frac{P_2}{P_1} = 1 + \frac{2\gamma_1}{\gamma_1 + 1} \times (M_s^2 - 1) \tag{1.1}$$

$$\frac{P_3}{P_4} = \left[1 - \frac{\gamma_4 - 1}{2}\left(\frac{u_3}{a_4}\right)\right]^{\frac{2\gamma_4}{\gamma_4 - 1}} \tag{1.2}$$

Since we have $P_2 = P_3$, combining eqn. 1.1 and eqn. 1.2, we get,

$$\frac{P_4}{P_1} = 1 + \frac{2\gamma_1}{\gamma_1 + 1} \times (M_s^2 - 1) \times (1 - \frac{(\gamma_4 - 1)a_1}{(\gamma_1 + 1)a_4} \times M_s^2) \tag{1.3}$$

where:

- $P_4$ and $P_1$ are the pressures of driver and driven section, respectively
- $P_2$ and $P_3$ are the pressures after the shock and expansion wave, respectively
- $u_3$ is the velocity of contact surface of driver and driven gases after the shock
- $M_s$ is the shock wave Mach number
- $\gamma_1$ and $\gamma_4$ are the ratios of specific heats of the driver gas and the test gas, respectively
- $a_1$ and $a_4$ are the sound of speeds of the driver gas and the test gas, respectively

## 1.5 Problem Statement

Supersonic shock tubes are widely used in Aerospace engineering for testing and validating CFD models, simulating hypersonic flow conditions, and studying the behavior of materials under extreme conditions. A supersonic shock tube facility with flow characterization capability can be used to produce shockwave of known properties to perform such studies.

## 1.6 Objectives

### 1.6.1 Main Objective

To determine the velocity characteristics of piston-driven shock tube with Mach behavior.

### 1.6.2 Specific Objectives

1. To design and fabricate a piston-driven shock tube.
2. To measure the pressure timeline on the wall of the shock tube.
3. To determine the flow Mach number from diaphragm burst pressure.
4. To determine Mach number by using ToF.
5. To characterize the shock tube for different X/L ratios.

## 1.7 Scope

After completion of this project, it can be used in many areas for different tests and projects. Among them, some are summarized below:

1. Experimental Verification

   This shock tube can be used for the verification of the various CFD simulations of shock behaviors.

2. Material Testing

   This shock tube can be utilized to examine the strength and behavior of materials under shock-induced conditions.

3. Experiments in Hypersonic Condition

   The flow from the tube can be attached to a C-D nozzle setup to generate hypersonic conditions for laboratory experiments.

## 1.8 System Requirements

### 1.8.1 Hardware Requirements

The hardware required for the completion of the project are listed below:

1. NPP-301B-700AT pressure transducer
2. AD620 amplifier module
3. NI USB DAQ X-series
4. High Speed Camera and Schlieren Setup
5. Machining tools (Lathe, Mill etc.)

### 1.8.2 Software Requirements

The software required for the project completion are listed below:

1. Programming Language: MATLAB
2. Design software: CATIA
3. Simulation software: OpenFOAM
4. Data Acquisition and Analysis: LabVIEW
5. Image Processing and Visualization: Image J, ParaView

# CHAPTER TWO:
# LITERATURE REVIEW

A free-piston shock tube is a type of shock tube facility used to generate high-speed shock waves for various experimental studies. It is called “free-piston” because the piston that compresses the driver gas is not mechanically linked to the external power source, but rather relies on the energy stored in the compressed air to drive the piston and generate the shock wave. Although the fundamental principle of a shock tube remains the same, the specific design and construction details can vary significantly depending on the intended application[3]. For examples, the paper entitled “Diaphragm construction for free piston shock tube/tunnel”[4] utilizes diaphragm construction having multiple rupture area. The provision of multiple rupture areas facilitates construction of the diaphragm from thinner material and quicker opening in comparison to single opening diaphragm. It uses both stainless steel and mild steel are for the fabrication of a shock tube [4]. Similarly, [5] employs doubled diaphragm system to push a piston that compresses the driver gas in high pressure. Another method to generate high pressure and high temperature involves compressing a light gas like helium to induce high velocity[6]. The paper titled as ”Design and fabrication of supersonic shock tube capable of producing shock waves uses stainless steel for the shock tube components fabrication [7]. There are multiple ways to achieve the desired output in a shock tube, such as modifying the diaphragms, piston, gases, and gas features. The design and manufacturing process can be optimized by carefully selecting the target outcome, requirements, and cost considerations.

Shock wave velocity has been measured using a variety of techniques. Probe techniques, the (TOF) Time of Flight Method, microwave reflection/Doppler method, luminous gas, dynamic calibration, and many more are examples of these methods. The Doppler method involves exciting a suitable microwave mode and frequency in a shock tube of circular cross section and detecting the wave pattern reflected by the ionized shock front.[8][9] This allows the absolute velocity of each shock to be measured and variations in velocity along the tube to be detected [8] . The microwave Doppler technique is suitable for high Mach number shock waves, where stronger shock attenuation near the end wall leads to varying shock strengths. Additionally, the microwave interferometer can be effectively used in an all-steel shock tube to measure electron density behind the incident shock, allowing for the study of impurities’ influence on the shock[9].

Several optical and laser methods are also employed for measurement purposes. For example, in the article by Medhi ”Time-resolved quantitative visualization of complex flow field emitted from an open ended shock tube using a wavefront measuring camera”,in the experimental velocity computation,the flow field was captured at different times using a Wavefront camera[10]. Using the 4F optical technique, flow field images are taken in separate, identical tests (one image at a time) by activating the camera unit at various times during the first 300 ms of the flow’s evolution following the shock discharge from the ST [10]. Probe techniques and Hall current measurements are additional methods used to calculate shock wave velocity. The study ”Dynamic Calibration Method of Blast Pressure Pencil Probes Based on Adjustable Shock Tube” [11] and oth-

ers utilized blast pressure pencil probes to investigate dynamic calibration techniques.

Patrick Gnemmi et.al [12] used Kulite transducers to measure pressure in various locations, including the nozzle exit, pitot pressure in the flow field, and surface pressure on models, in their paper "Overview of activities at the ISL Hypersonic Shock Tunnel." The pitot-pressure measurements were performed using a rake equipped with 11 Kulite piezo-resistive pressure transducers [12]. This sensor is used in conjunction with other measurement techniques, including high-speed visualization, heat flux measurement, and particle image velocimetry [12]. The Kulite pressure transducer is also utilized in the supersonic ejector facility at the Laboratory for Hypersonic and Shock Wave Research for pressure calibration [13]. The system has utilized a piezo resistive PCB-123 pressure transducer to monitor and calibrate pressure shocks, ensuring accurate measurements of the pressure arrival times [14]. Researchers at IISc have developed and calibrated fast-response MEMS sensors for surface measurements in the Hypersonic Shock Tunnel (HST-2). The sensors are designed to operate within the typical test time of 600 microseconds, enabling precise measurements in the hypersonic environment [15].

The precise placement and mounting of pressure sensors are major requisite for accurate pressure calibration, as they directly impact the reliability of the measurements. The paper titled "Description of the shock tube and comparison of flush mounted and recess mounted pressure sensors" showed that the difference of comparison of flush mounted and recess mounted pressure sensors[16]. Degree of contact between sensor and material may have a significant effect on results. This paper said that however, any cavity such as the 2 mm recess limits the frequency content of any signal that passes through the cavity, The rapid rise in pressure at all sensors when the endplate was uncovered suggests that many frequencies above this level were part of the shock wave. Thus, a recessed sensor may not read the correct pressure values. Flush mounted provided better results in comparison to the recess mounted[16] [17].

Placement of pressure sensors enables us to properly calculate the properties of flow overall the tube. The literatures suggested that proper placing of pressure sensors is mostly done by placing the sensors near diaphragms to calibrate the shock properties. 4 pressure transducers were utilized to calibrate, 2 incident side on to measure pressure on sides walls and 2 on end wall is used to calculate the end wall pressure [17].The paper entitle "Test Gas Slug Characterization for Large-Scale Shock Tube Facility" presented that Hypersonic Shock tunnel-2(HST-2) at IISc Bangalore utilizes three pressure transducers, one at end wall and 2 at side wall, 40mm and 380 mm away from end wall [18]. Similarly, HST-4 also utilizes three pressure transducers, one at end wall and 2 at side wall 234mm and 480mm away from end wall . This shows that the placement of transducers depends upon the tube internal diameter and length[18].

In the study of shock wave generation and behavior, understanding the dynamics of diaphragm rupture and shock interactions is essential. When the incident shock impacts the diaphragm, its motion is initially restricted due to boundary clamping, forming a weak transmitted precursor shock. The strength of this precursor decreases with increasing diaphragm mass. As the diaphragm stretches, fails, and accelerates downstream, a stronger second shock forms and overtakes the precursor shock. Heavier

diaphragms take longer to accelerate, delaying the catch-up time and strengthening the second shock due to persistent reflected shock conditions. In contrast, lighter diaphragms accelerate faster, generating a stronger upstream expansion that weakens the reflected shock and delays its arrival at the transducer[18].

Various materials are employed to investigate shock wave generation in shock tubes, where the diaphragm's material, combination, and thickness play a crucial role in controlling the pressure difference and resulting shock properties. The material must have sufficient strength to endure the applied pressure. Some of the materials include Aluminium foil, Mylar (Biaxially-oriented Polyethylene terephthalate).[19] found that 95 GSM tracing paper was the most durable reinforcing material, followed by 75 GSM royal executive bond paper and standard 70 GSM paper when used with aluminum foil diaphragms. Additionally, the combination and arrangement of materials notably enhance the Mach number of the generated shock wave and its precision.[20]

To store and analyze data from sensors, a data acquisition system is necessary. Various types of data acquisition systems are designed and calibrated. For instance, [21], used the NI USB-6351 model, an X-Series Data Acquisition device, to digitize signals through analog-to-digital conversion for data acquisition . The LabVIEW application software with the NI-DAQ mx driver software is installed on the computer as a platform for visual programming. This software includes tools to configure, acquire data, and send data to DAQ devices[21][22]. Additionally, data acquisition systems can be developed in-house using open-source hardware and software platforms like ARDUINO and PROCESSING for cost-effectiveness[23] .

In the field fluid dynamics and shock wave analysis, optical visualization techniques play a crucial role in understanding complex flow phenomena. The single-mirror schlieren setup is a simplified optical method for visualizing fluid density variations caused by shock waves and thermal gradients.[24] It replaces complex multi-component systems with a single concave mirror, reducing alignment challenges and optical aberrations. Light from a point source is collimated by the mirror, passes through the test section, and refracts due to density gradients. The refracted rays return to the mirror and are focused onto a knife edge, which selectively blocks portions of the light, creating contrast between bright and dark regions. A camera captures this pattern, clearly visualizing shocks, turbulence, or other flow features. This system is particularly effective for high-speed flows and scalable for larger test sections.[25]

Much of the earlier literature on droplet breakup consists of experimental work performed in shock tubes and wind tunnels. Normal shock waves, by themselves, have little effect on the droplet. However, they have proven to be a reliable and repeatable technique to generate a high-speed flow around the droplet, which is responsible for the deformation and disintegration.[26]. The action of air friction and pressure causes the deformation of drops and ligaments which subsequently break up in the relative airflow. It seems generally agreed that this always occurs, regardless of whether the liquid jet enters still air at high speed, or whether a low-speed jet of liquid interacts with a faster airflow [27].The varying morphologies in the droplet breakup process for shock tube studies are generally presented by means of deformation, breakup and secondary atomization, depending on the droplet size and flow conditions [26].

# CHAPTER THREE:
# METHODOLOGY

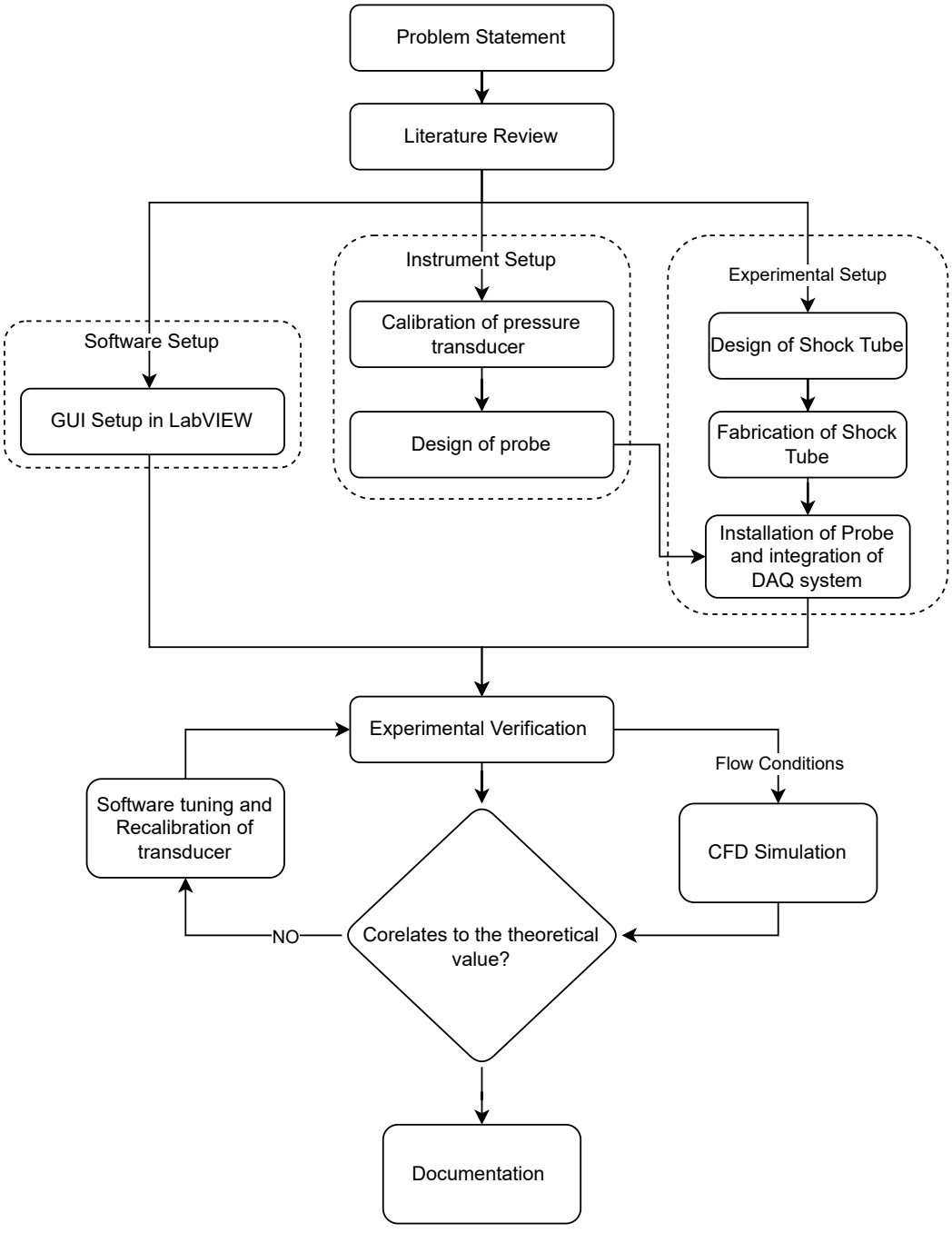


Figure 3.1: Methodology Flowchart

## 3.1 Experimental Setup

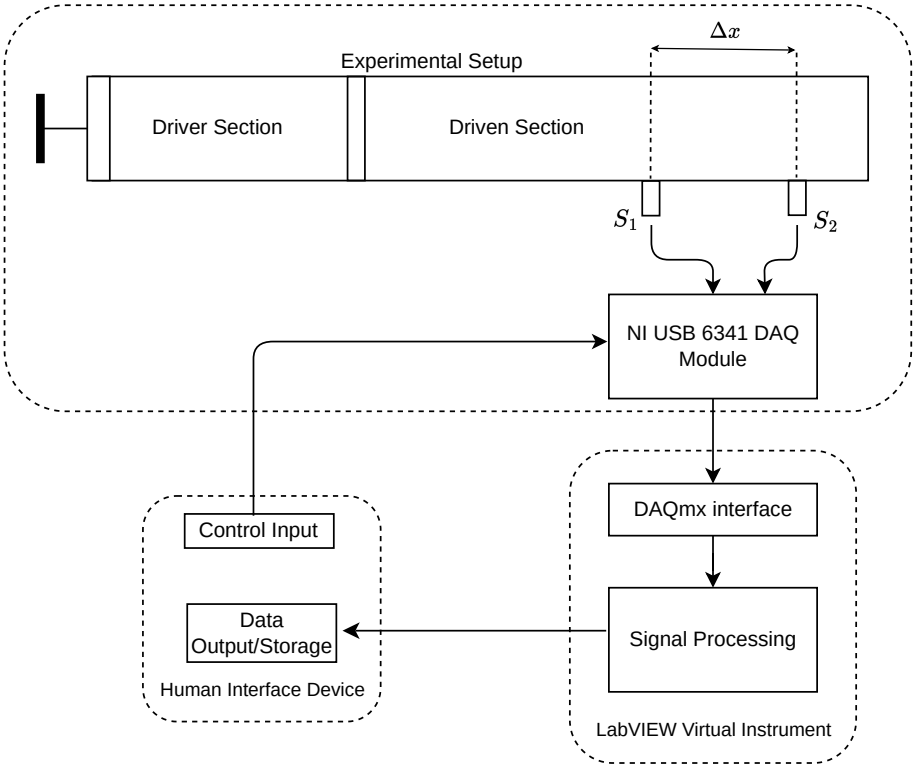


Figure 3.2: Experimental Setup

## 3.2 Design of Shock tube

Different operational and effective shock tube were reviewed for reference. Based on the mode of operation, required experimental conditions, and the scale of the facility to be developed, a free piston design was selected. The design of shock tube is inspired from Reddy Tube [28]. A shock tube was designed with dimension of 490 mm for driver section and 510 mm for driven section. The internal diameter of the shock tube is 29 mm and external diameter is 47 mm. It was fabricated with two M12 threaded holes within the driven section for the pressure probe placement.

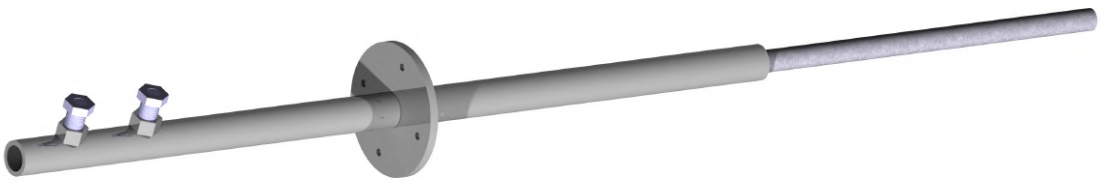

Figure 3.3: CAD design of shock tube.

### 3.2.1 Diaphragm Material

Previous work on the shock tube involved using various diaphragm materials, including aluminum foil, Mylar, Royal Executive Bond paper, tracing paper, and cellophane paper. Aluminum foil with a thickness of 18 microns was selected as the diaphragm material due to its easy availability and the accessibility of burst pressure data from prior experiments. To achieve a higher pressure ratio, multiple layers of aluminum foil were used as diaphragms.

### 3.2.2 Placement of Probes

The fabricated shock tube featured two cavities in the driven section designed for probe placement. These probes are strategically placed 100 mm apart from each other at 70 mm from end of the driven section to measure pressures essential for flow analysis.

## 3.3 Fabrication of Shock tube

The shock tube was fabricated using SS material. 28×47 seamless SS tube was used for fabrication. The internal surface of driver tube was honed down to 29 mm diameter using lapping paste for smooth internal finish resulting in repeatability. SS flanges of thickness 5 mm were welded on both section for diaphragm placement.

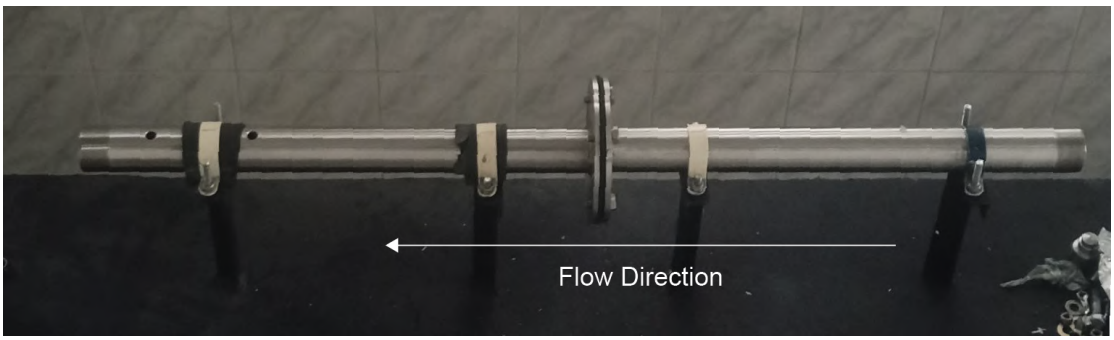


Figure 3.4: Fabricated Shock tube

For the hand-driven piston shock tube, the piston was fabricated using MS rod and a 29-16-7 oil seal was fixed on the end of the piston using M8 bolt for sealing.

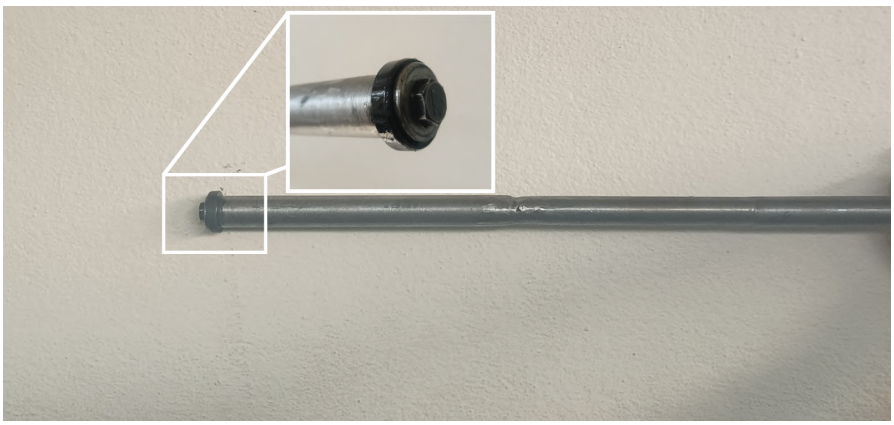

Figure 3.5: Piston

## 3.4 Pressure Measurement Device

A probe was required to measure pressure at different locations within the tube. The probe must meet following criteria:

- High frequency response for capturing rapid pressure change.
- Accurate and precise pressure measurement to ensure reliable data.
- Least disturbance to the flow inside the tube.

### 3.4.1 Pressure Transducer

The pressure transducer measures the pressure changes caused by the shock wave propagation through the tube. These transducers were typically located at known positions along the tube and were flush mounted to the inner wall of the tube. Being exposed to the shock wave, they sensed the shock front as it passes by, providing information about the pressure and its variations during the shock wave propagation. The pressure measurement system comprised of a pressure sensor and a voltage amplifier. The pressure sensor measures the rapidly changing pressure, whereas the amplifier is used to amplify the output signal from the pressure sensors.
A piezo-resistive pressure transducer, NPP-301B-700AT, from Amphenol Novaseries was paired with the AD620 amplifier module with gain up to 1000 times for the input reading of voltage, which was connected further to the NI DaQ X Series 6341 for pressure reading.
The dimensions and response rate of the transducer matched the requirements of the project. The dimensions of the transducer are shown in figure 3.6. The specification of the selected transducer is presented in the table 3.1 .

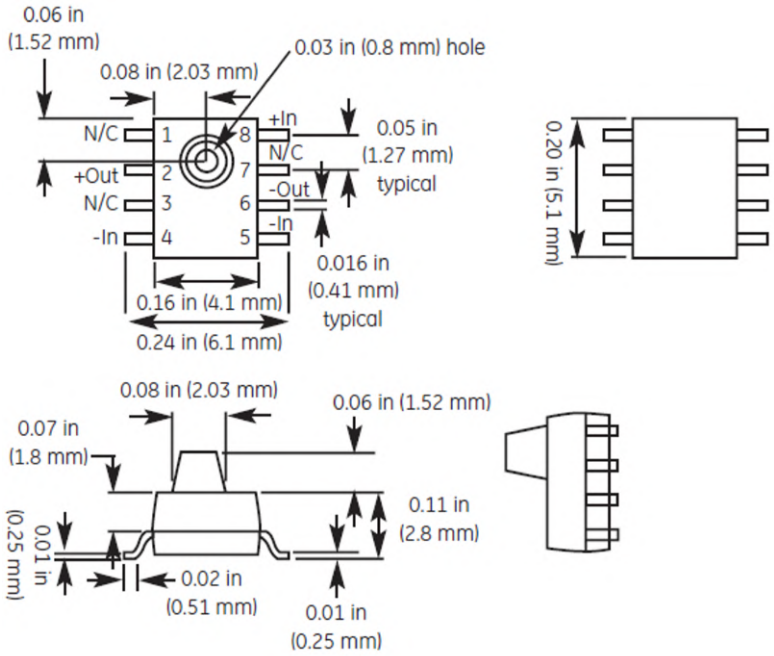


Figure 3.6: NPP-301 Pressure Transducer

Table 3.1: Specifications of NPP-301B-700AT pressure transducer

| Parameter | Value |
|---|---|
| Pressure Range | 100 kPa |
| Maximum Pressure | 3 ×rated Pressure |
| Operating Temperature | - 40 °C to 125°C |
| Full Scale Voltage Output | 60±20 mV |
| Linearity | ±0.20% FSO |
| Response time | 250µs |

### 3.4.2 Transducer PCB Design

PCB mounting enables a transducer to be securely attached to a structure. A two-layer PCB was designed for mounting NPP-301B-700AT pressure transducer. The back side of the PCB features pads for soldered wire connections, as well as pads for surface-mount compensating resistors. The PCB design facilitates compensating resistance on one of two legs, whichever recommended by the balancing formula.

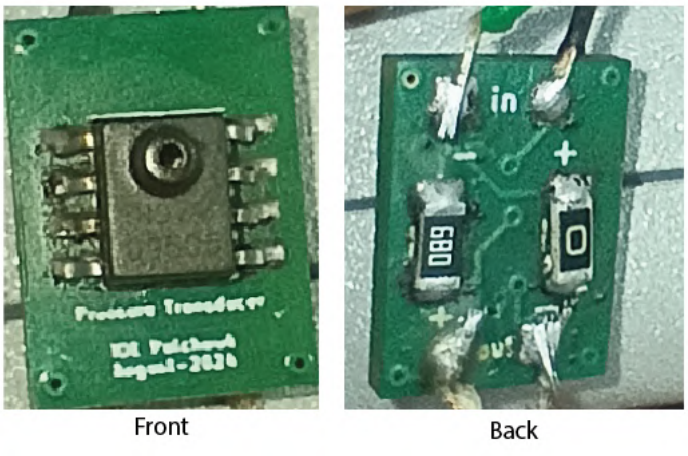


(a) Assembled PCB

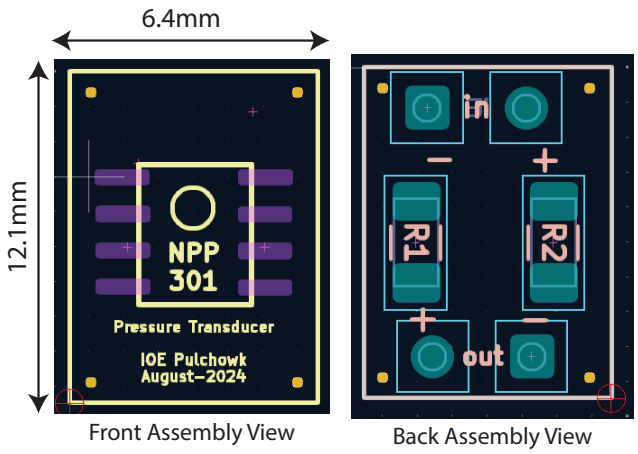


(b) Design in Kicad

Figure 3.7: PCB for pressure Transducer

### 3.4.3 Amplifier Connection and DAQ System

The PCB is connected to AD620 amplifier module for signal conditioning, which is then connected to NI-USB 6341.

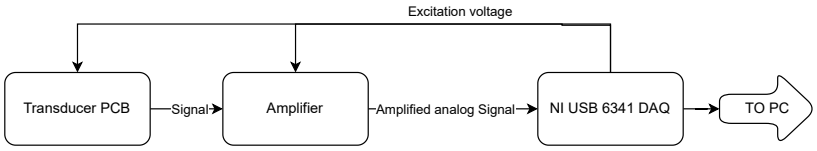


Figure 3.8: Pressure transducer system schematic

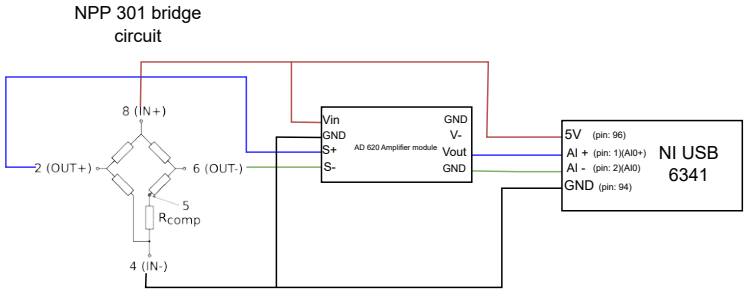


Figure 3.9: Circuit connection of pressure measurement device

### 3.4.4 PCB Design for amplifier connection

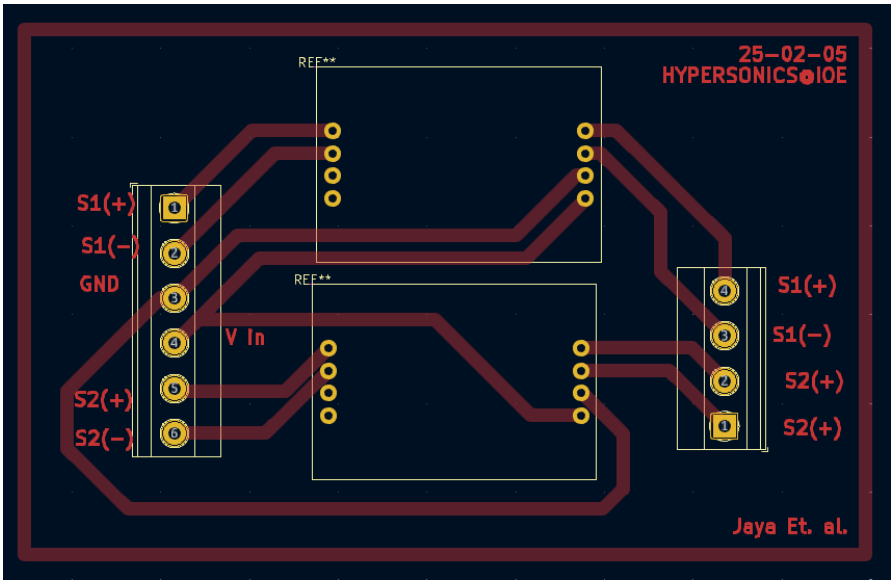


Figure 3.10: PCB Design for amplifier connection

The circuit diagram represents the connection of Amphenol NPP-301B-700AT transducer to an AD620 instrumentation amplifier, ensuring proper signal acquisition and amplification before interfacing with a DAQ (Data Acquisition) system.

### 3.4.5 Calibration of Pressure Transducer

The dump tank of the shock tunnel was used as vacuum chamber for the calibration of pressure transducer. An acrylic lid was designed to fit on the nozzle opening of the dump tank to facilitate the passage of wire. Voltage readings from the transducers were recorded at various pressures and the two values were fit linearly to get the values of slope and intercept.

Table 3.2: Calibration of Transducers

| Gauge reading (mmHg) | Absolute Pressure (Pa) | $V_{Transducer1}$ | $V_{Transducer2}$ |
|---|---|---|---|
| 0 | 87368.83 | 0.096 | 0.362 |
| -100 | 73768.83 | 0.007 | 0.241 |
| -200 | 60168.83 | -0.095 | 0.176 |
| -300 | 46568.83 | -0.203 | 0.088 |
| -400 | 32968.83 | -0.265 | 0.012 |
| -500 | 19368.83 | -0.388 | -0.084 |
| -600 | 5768.83 | -0.478 | -0.153 |

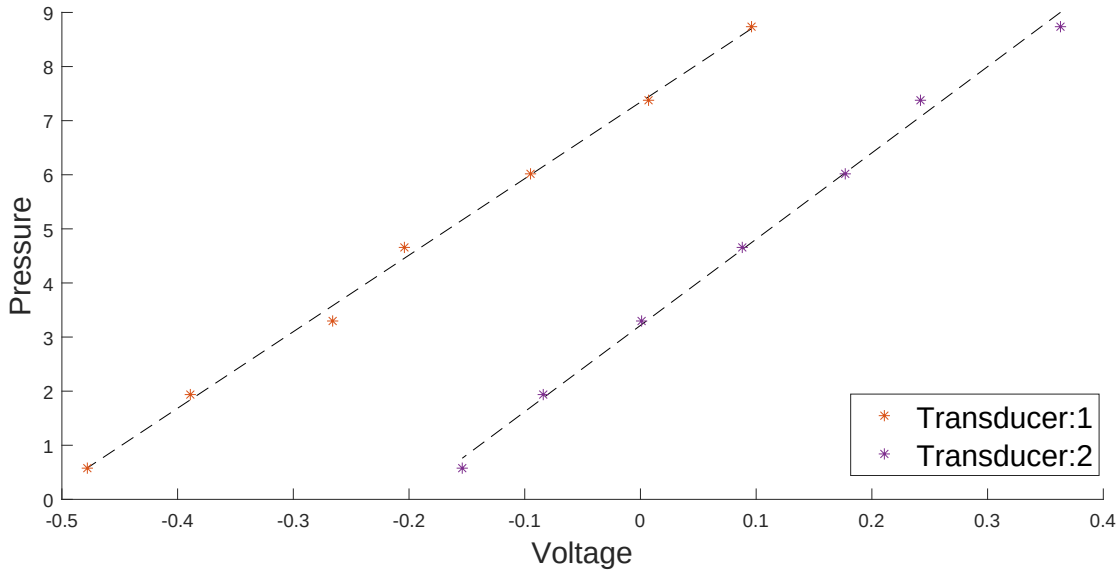


Figure 3.11: Voltage vs Pressure for transducers

Table 3.3: Calibration Values for two transducers

| Transducer | Slope | Intercept |
|---|---|---|
| 1 | 146135.4455 | 72755.2854 |
| 2 | 170269.9358 | 32882.4506 |

## 3.5 Data Acquisition System

NI X Series USB 6341 DAQ system was used as the interface between the transducers and LabVIEW[29] software for the pressure measurement. The specifications of

interest are as follows:

Table 3.4: Specifications of NI USB-6341 DAQ

| Specifications | Data |
|---|---|
| **Sample rate** | |
| Single channel maximum | 500 k Sample/s |
| Multichannel maximum (aggregate) | 500 kSample/s |
| Minimum | No minimum |
| Timing resolution | 10 ns |
| Timing accuracy | 50 ppm of sample rate |
| Input coupling | DC |
| Input range | ±0.2 V, ±1 V, ±5 V, ±10 V |
| Maximum working voltage for analog inputs (signal + common mode) | ±11 V of AI GND |
| Scan list memory | 4,095 entries |
| Data transfers | USB Signal Stream, programmed I/O |

### 3.5.1 LabVIEW Setup

For the LabVIEW Setup, the NI USB 6341 DaQ module was first connected to the device where LabVIEW was installed. In LabVIEW block diagram, DaQ assistant was imported and the signal were acquired from respective channels, the number of samples of data and its rate were also defined. Also, the data was logged in '.tdms' format.

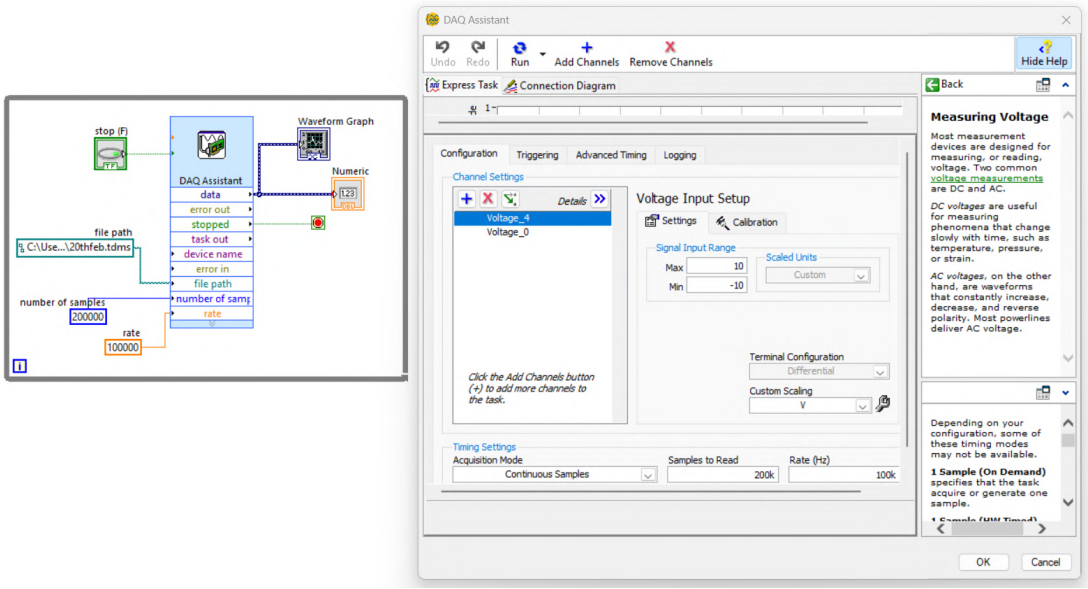


Figure 3.12: Block diagram of data acquisition in LabVIEW VI

**DAQmx Configuration**

- Sampling Rate: 100Ks/S
- Acquisition Mode: Continuous Mode
- Terminal Configuration: Differential
- Buffer Size: 200Ks
- Logging: saved to specified .tdms file

The logged tdms file was post processed using MATLAB. Mach number was calculated using Time of Flight method with the help of delay in pressure rise in readings of transducers.

**Time of Flight Method**

The time shock wave takes to travel between two points is typically measured by placing sensors or probes at known distances along the shock tube. The time difference between the shock wave detection at two points is used to calculate the shock velocity. This method is called Time of Flight.
Two pressure transducers placed 100 mm apart are used for ToF calculation of shock wave mach number.

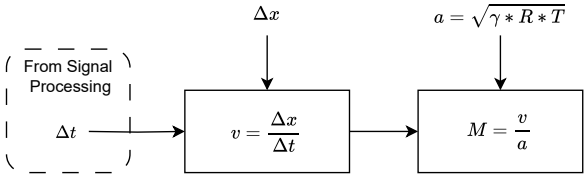


Figure 3.13: Mach number calculation by ToF

## 3.6 Schlieren Setup

For the visualization of shock wave formed in the shock tube, a single mirror Schlieren was used. The Schlieren setup consisted of a spherical concave mirror, a point light source setup with a knife edge, and a high-speed camera. The experiment utilized a concave mirror with a focal length of 1200 mm and a diameter of 112 mm. A Chronos 2.1 HD high-speed camera was used for capturing the shock wave. The point source and knife edge were positioned at 2f for Schlieren imaging. This setup was laid just at the outlet of the shock tube to observe the shockwave and flow patterns behind it at the end of a driven section.

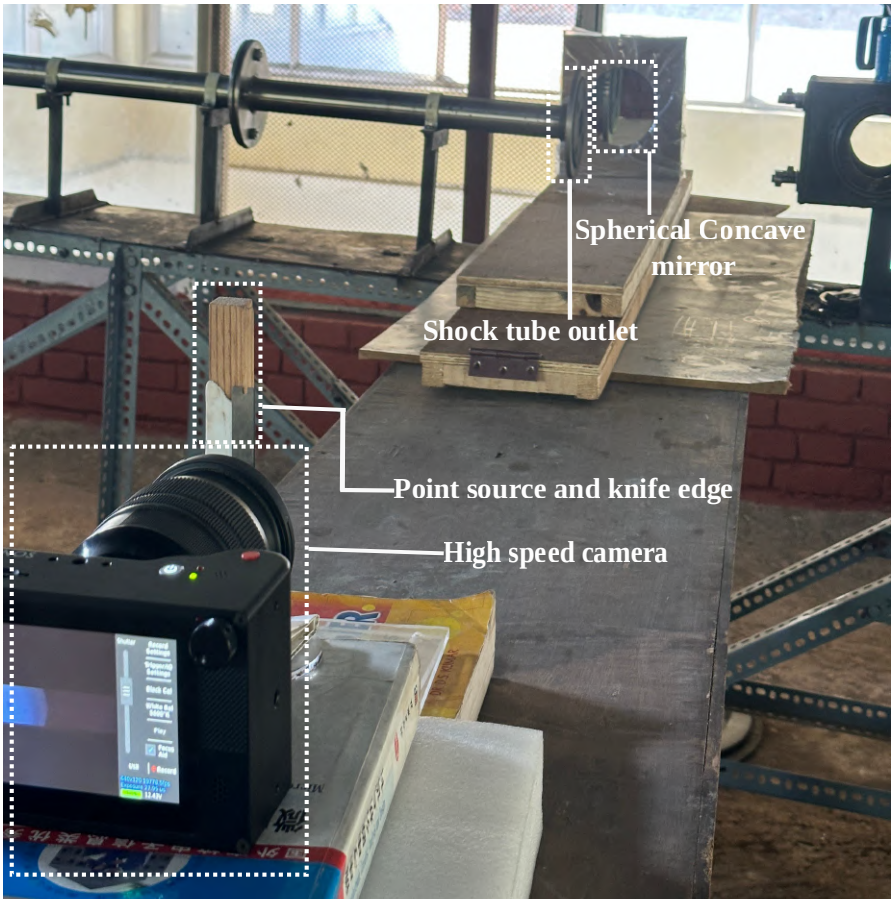


Figure 3.14: Schlieren Setup

# CHAPTER FOUR:
# RESULTS AND DISCUSSIONS

## 4.1 Shock Wave Visualization

A 0.072 mm thick aluminum foil diaphragm was used for the test of the tube. When the piston was manually pushed to x/l of 0.15 in the driver section, the pressure ratio reached the burst pressure ratio of 14.23. which led to the rupture of the diaphragm.

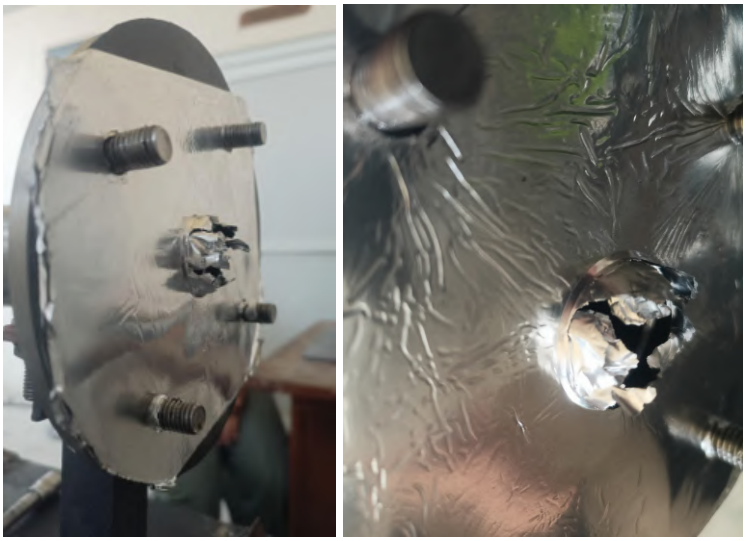

Figure 4.1: Diaphragm Burst

After the burst of the diaphragm, the shock wave traveled through the driven section and further from the open end of the driven section. This flow was visualized using single mirror Schlieren.

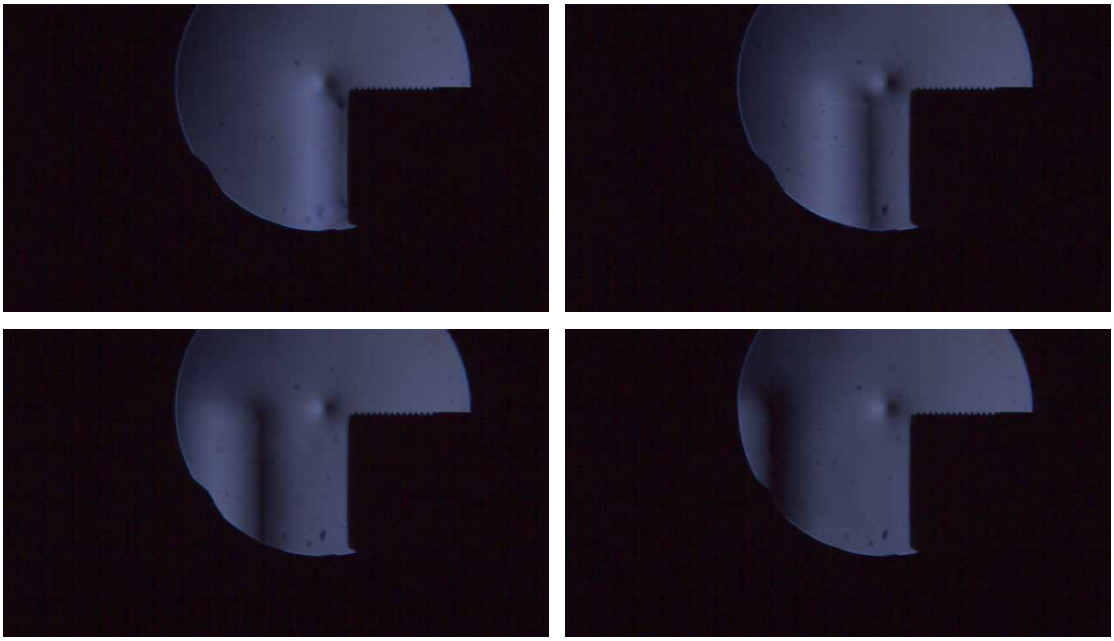

Figure 4.2: Schlieren Images of Pressure Waves downstream of Shock tube

## 4.2 CFD of Shock tube

The shock tube was simulated to validate the mach number of the shock generated from experimentally obtained burst pressure for different diaphragm thicknesss. The initial pressure and temperature for the driver and driven section were taken from the atmospheric condition when the experiment was conducted. This was done in 3D geometry of the actual model of the fabricated tube. The case was set up for the piston-driven environment for which the driver section length is suitable for the particular burst pressure taken from *x/l* ratio. The ToF method was used in the simulation for velocity measurement, where two sensors were placed at a known place. This was done using the viscous pressure based transient solver *rhoPimpleFoam* of OpenFoam software for a more realistic nature of flow inside the tube. The results obtained from the simulation were visualized using open-source software ParaView.

### 4.2.1 Geometry

The domain for the simulation were made to replicate the piston-driven environment for an actual shock tube. The domain was a 580 mm long cylindrical tube which was made by 5 blocks with one block at the center and 4 blocks surrounding it along the circumference. The external diameter of the outer blocks was 29 mm. Only a small volume was pressurized with the obtained burst pressure when the piston was used, and the length of the driver section was set to 70 mm based on the *x/l* ratio. So, a cylindrical tube with a 70 mm driver section and a 510 mm driven section was simulated.

### 4.2.2 Mesh

Mesh for this project is created using the *blockMesh* utility of the OpenFOAM software. The mesh independence study based on the reflected pressure value for three different meshes determined the number of grids for the meshing in all directions. A coarse, medium, and refined mesh were created, each with the cell number increasing by $\sqrt[3]{2}$ times. Using Richardson extrapolation technique and relative error method [30], mesh independence study was done to fix the discretization of the domain for this problem.

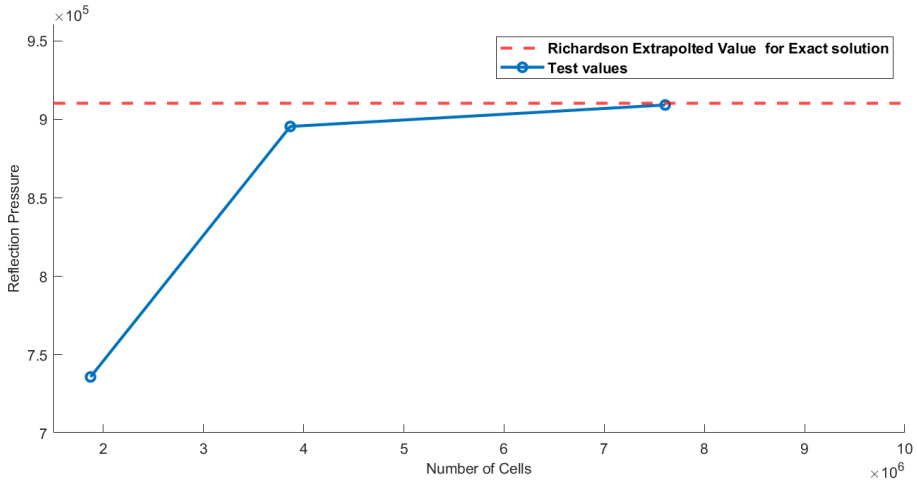


Figure 4.3: Plot of Test values of Inlet pressure to Number of Cells.

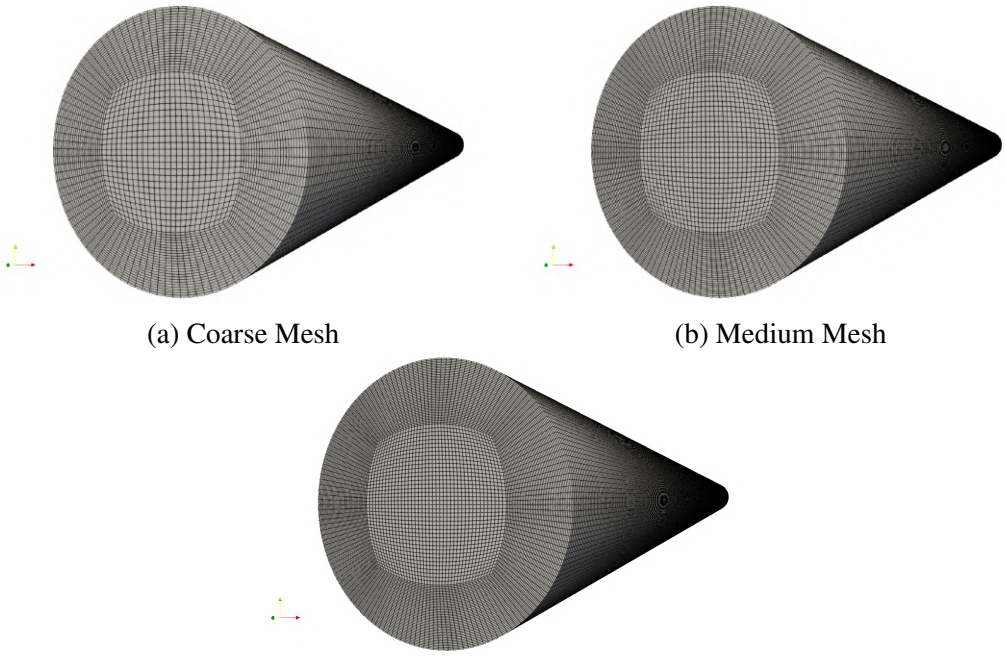

(a) Coarse Mesh

(b) Medium Mesh

(c) Fine Mesh

Figure 4.4: Meshes chosen for Mesh Independence Study

Table 4.1: Relative Error of Test Reflection Pressure With Richardson Extrapolated Value

| Mesh | No of Cells | Test value of Reflection Pressure | Relative Error(%) | GCI(%) |
|---|---|---|---|---|
| Coarse | 1871875 | 735965 | 19.164 | - |
| Medium | 3865600 | 895492 | 1.642 | 19.812 |
| Fine | 7608000 | 909164 | 0.14 | 1.644 |

The data obtained from the grid independence test is given in the above table 4.1. The grid convergence index between medium mesh and fine mesh was found to be 1.644, which is the acceptable value. Also, the relative error value of the extrapolated value of reflected pressure and the reflected pressure value from simulation have a relative error of 0.1408% which shows that this fine mesh has little chance of error. Hence, a finer mesh configuration with 7608000 cells was chosen for the study. Here the domain was divided into 40 grids in the x and y directions, and 951 grids in the z direction for all the blocks.

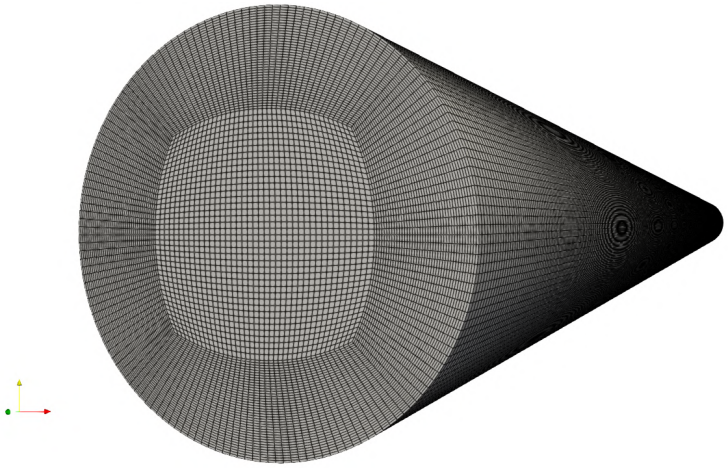

Figure 4.5: Final Mesh Selected

The simulation domain was divided into high-pressure and low-pressure cylindrical sections using the *setfield* utility available in OpenFOAM. For the driver section, a pressure of 1.33 *MPa* which was a burst pressure obtained from the experimental data of *x/l*.

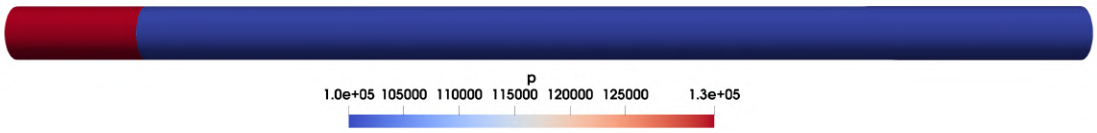


Figure 4.6: Compressed driver gas initial condition for CFD

### 4.2.3 Boundary Conditions

For analysis, two ends of the tube were specified as *patch* and a necessary boundary condition for reflection was allocated. For this patch, pressure and temperature boundary condition were set as *zeroGradient* with a uniform velocity of zero m/s. The circular surface of the cylinder was given a wall boundary condition with pressure, velocity, and temperature behaviors near the wall.

### 4.2.4 Outcome and discussion of results from simulation

The simulation was run from 0 to 0.002 sec where the time step was 5e-6 sec. Since the pressure transducer and ToF method were used for the mach calculation, two probe points were created, the same as in the fabricated tube, and the pressure versus time plot at that time was recorded. From the time difference between the sensing of pressure between those two points, the mach value was calculated. For diaphragm burst pressure of 1.33*MPa*, the flow mach number was 1.7537.

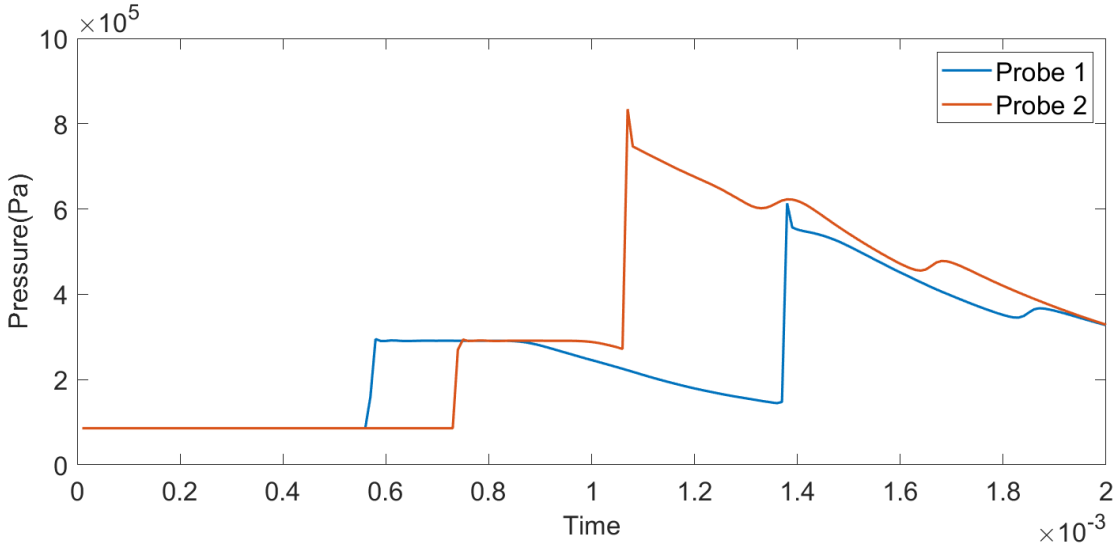


Figure 4.7: Pressure vs time at probe locations

## 4.3 Pressure Characterization

### 4.3.1 Burst Pressure Characterization for different *x/l* ratios

The compression ratio was recorded for different numbers of layers of aluminum foil, used as the diaphragm, and the burst pressure ratio was calculated using adiabatic gas relations.

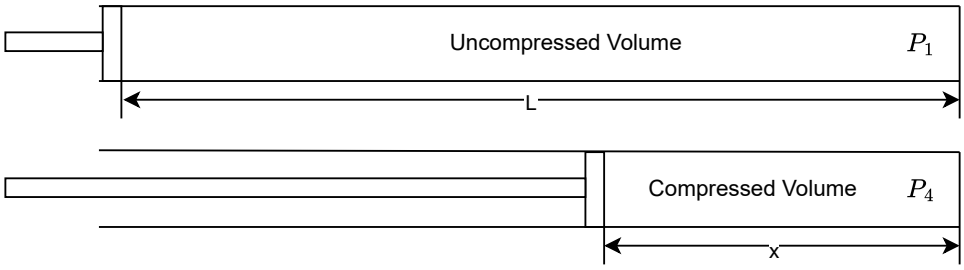


Figure 4.8: Piston inside driver section of shock tube

$$PV^{\gamma} = constant$$
$$P_1 V_1^{\gamma} = P_4 V_4^{\gamma}$$
$$or, P_1 (Al)^{\gamma} = P_4 (Ax)^{\gamma}$$

simplifying, we get,

$$\frac{P_4}{P_1} = (\frac{x}{l})^{-\gamma} \tag{4.1}$$

Multiple tests were carried out for different thicknesses of diaphragm to calculate the burst pressure ratio. A high speed camera was used to capture different frames while pushing the scaled piston. The piston motion was tracked from the frames and burst instance was determined from sudden acceleration of piston.

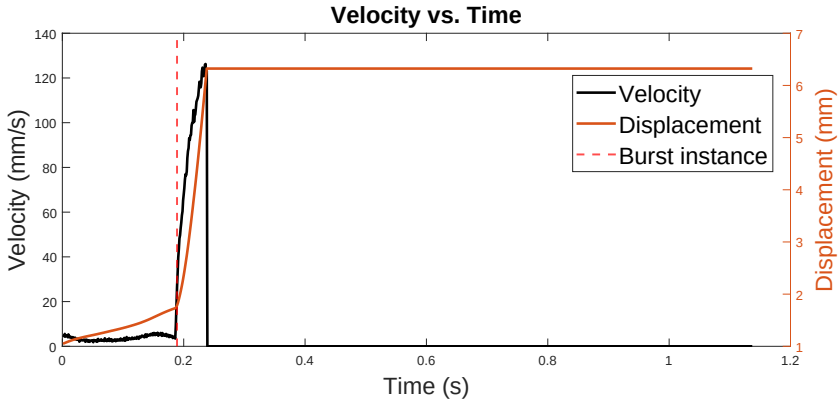


Figure 4.9: Piston motion vs time for 0.054 mm diaphragm

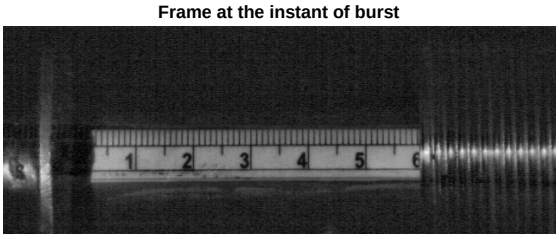


Figure 4.10: Frame of piston position during diaphragm burst

There is an uncertainty in the value of the compression ratio before burst due to the inability to stop the piston at the instant of burst. A median of burst pressure ratio values for maximum thickness diaphragm was taken as the initial condition for the simulation verification.
$\gamma = 1.4$
Total driver section length = 505 mm
Piston length = 462 mm

Table 4.2: Burst Pressure Characterization by *x/l* ratio

| No of Layer(s) | Diaphragm Thick-ness | x | *x/l* | $P_4/P_1$ |
|---|---|---|---|---|
| 2 | 0.036 | 157 | 0.314 | 5.062 |
| 2 | 0.036 | 160 | 0.32 | 4.929 |
| 3 | 0.054 | 106 | 0.212 | 8.773 |
| 3 | 0.054 | 110 | 0.22 | 8.329 |
| 3 | 0.054 | 114 | 0.228 | 7.923 |
| 4 | 0.072 | 85 | 0.17 | 11.95 |
| 4 | 0.072 | 75 | 0.15 | 14.239 |
| 4 | 0.072 | 79 | 0.158 | 13.24 |
| 4 | 0.072 | 84 | 0.168 | 12.15 |

The plot below shows a comparison in the experimental values to the theoretical value of pressure ratio calculated from the equation 1.3.

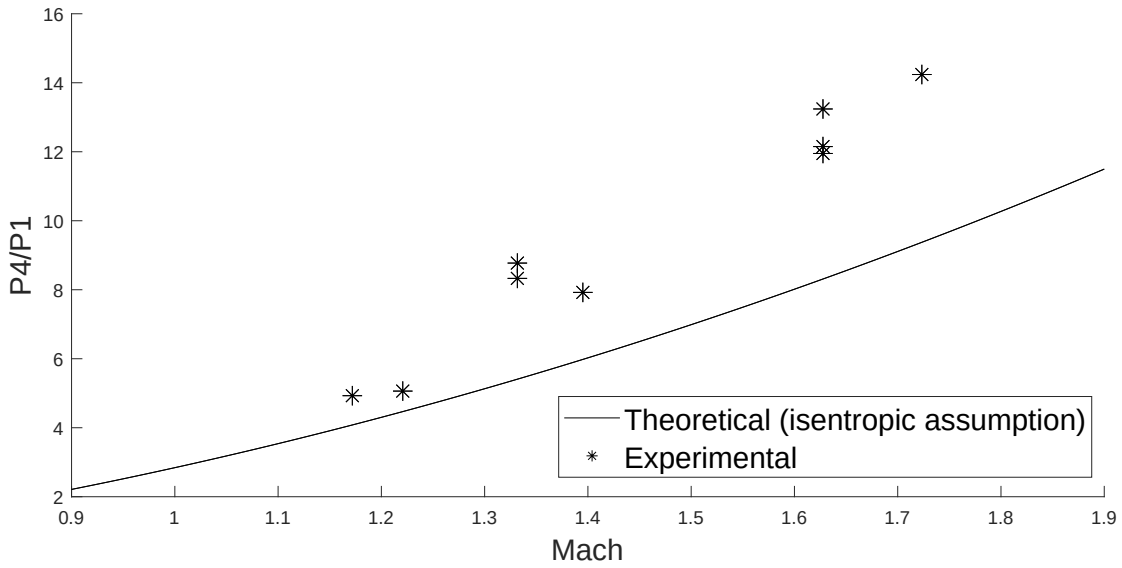


Figure 4.11: Mach vs Compression ratio

The variation in experimental burst pressure ratio from ideal could be due to the following reasons:

- Adiabatic assumption might not be valid in the driver section compression due to losses through the bolt in piston and wall of the tube.
- The aluminum diaphragm forms a convex surface when pressurized; this could increase the actual volume at end of compression and thus result in overestimation of pressure ratio[31].

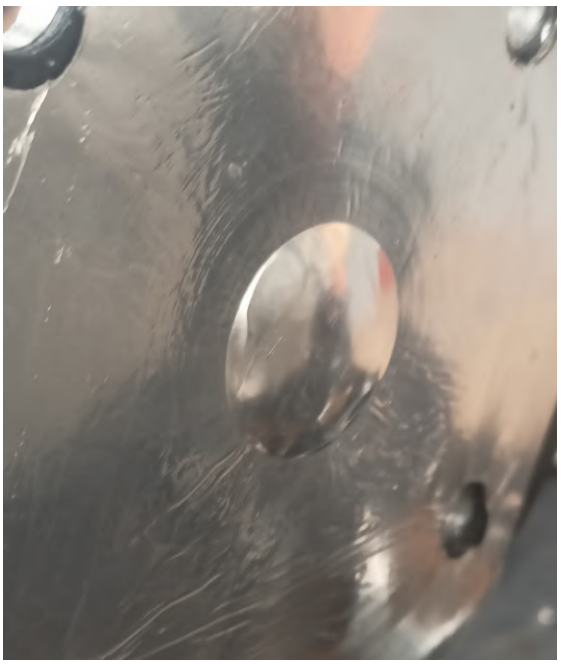

Figure 4.12: Formation of convex surface of diaphragm before reaching burst pressure ratio

### 4.3.2 Pressure timeline at wall of Shock tube

After the file was logged in LabVIEW, the measurement data were post-processed in MATLAB, showing readings of two transducers against time and were plotted.
Tests were performed with open-ended shock tube and with an end-plate to verify reflected pressure build up for application in shock tunnel.

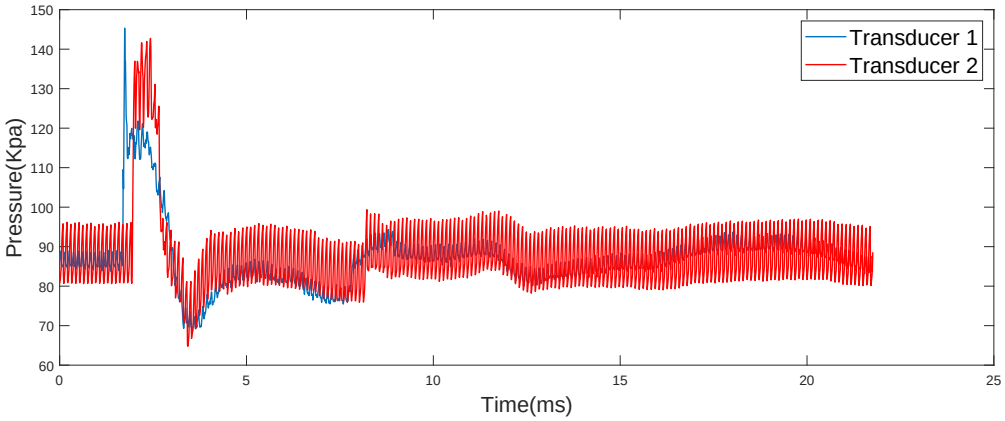


(a) Diaphragm Thickness=0.036 mm

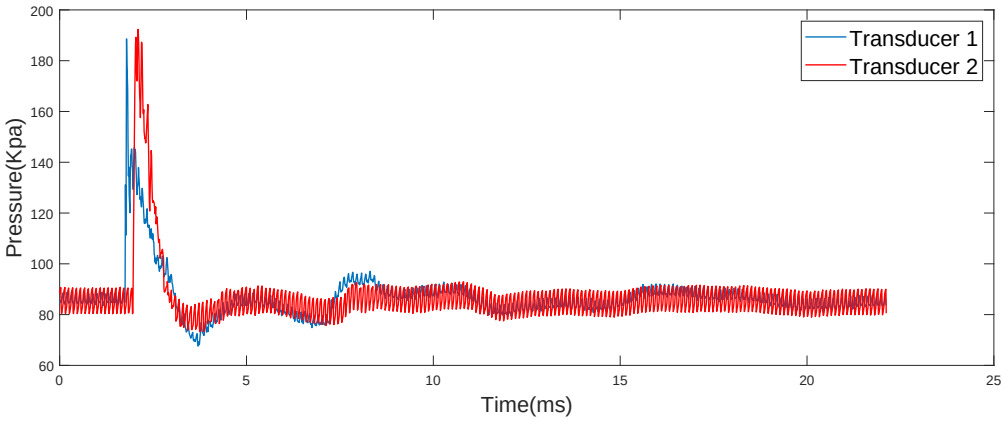


(b) Diaphragm thickness=0.054 mm

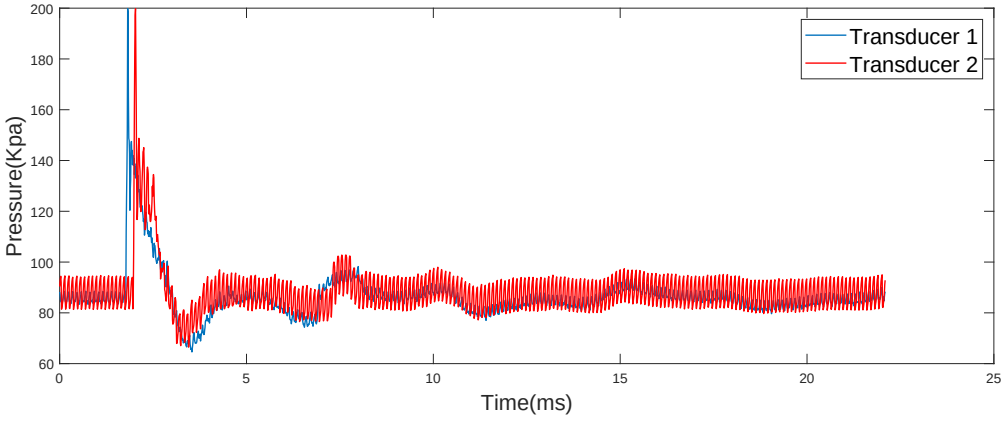


(c) Diaphragm Thickness=0.072 mm

Figure 4.13: Pressure timeline at probe locations

### Reflected Waves Pressure Distribution

Pressure characteristics of the shock tube with a 3 mm MS end plate installed at the end of driven section were observed and compared to CFD results with driver gas conditions taken from $x/l$ measurements.
The plots show the sudden rise in readings when the waves pass transducer 1 and then transducer 2, respectively. After hitting the end plate, the reflected shockwave, which further increases the pressure, is first read by transducer 2, and then transducer 1. This phenomenon is observed in the pressure timeline at transducer locations.

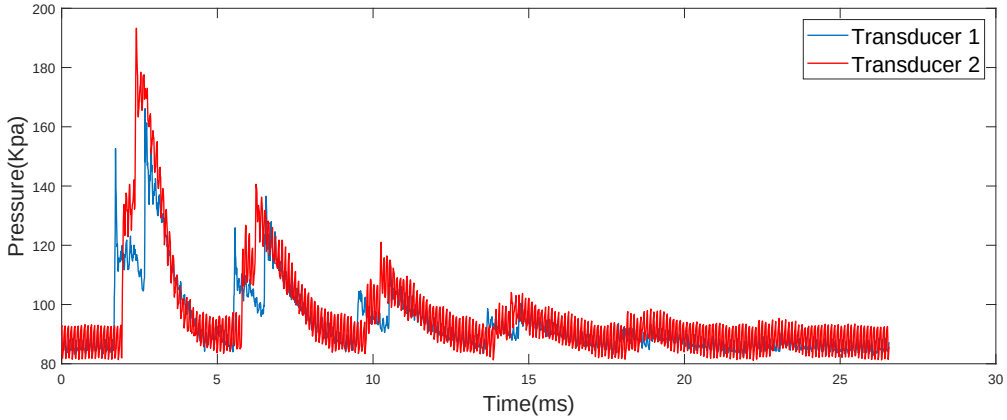


(a) Diaphragm Thickness=0.036 mm

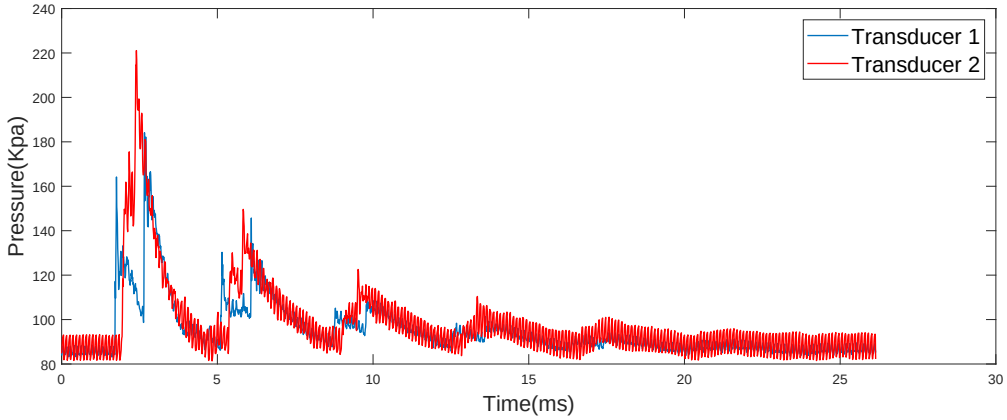


(b) Diaphragm thickness=0.054 mm

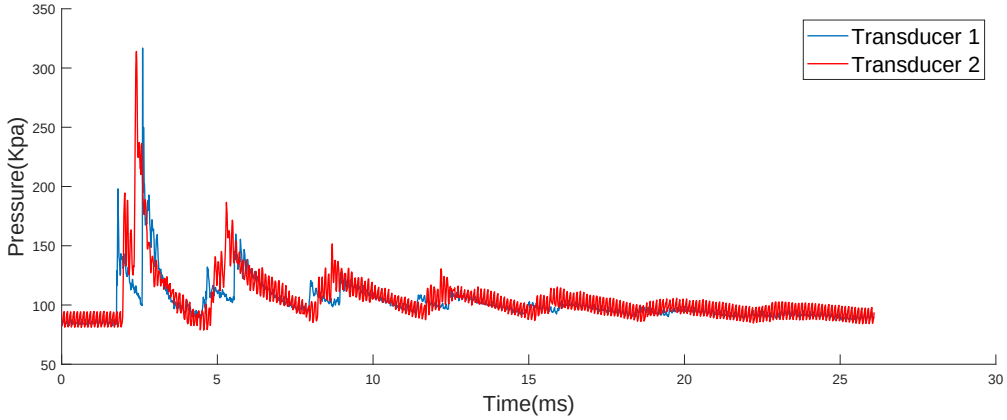


(c) Diaphragm Thickness=0.072 mm

Figure 4.14: Pressure timeline at probe locations with end-plate

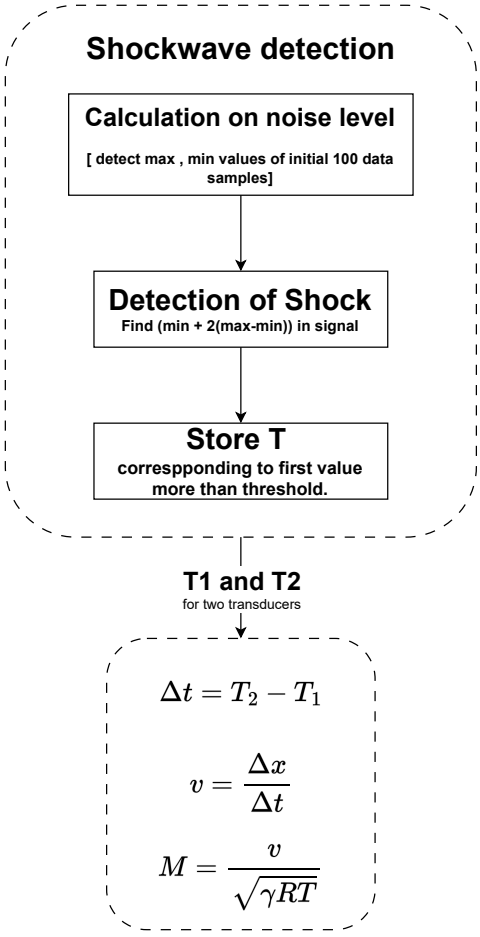


Figure 4.15: Signal Processing block diagram for mach calculation

## 4.4 Shock-Wave Mach Measurement

Time of Flight (ToF) method was used to determine the velocity of flow in the shock-tube.
The velocity paired with room temperature acquired from meteorological data was used to calculate the mach number of the shock.
Room Temperature = $20^oC$
Table 4.3 gives the mach character for different numbers of layers of 18 microns aluminum foil used as a diaphragm.

Table 4.3: Measured shockwave mach number at different diaphragm thickness

| No. of layer(s) | Diaphragm Thickness (mm) | Time Delay ($\mu s$) | Flow Velocity ($m/s$) | Mach Number |
|---|---|---|---|---|
| 2 | 0.036 | 240 | 416.667 | 1.221 |
| 2 | 0.036 | 250 | 400 | 1.172 |
| 3 | 0.054 | 220 | 454.545 | 1.332 |
| 3 | 0.054 | 220 | 454.545 | 1.332 |
| 3 | 0.054 | 210 | 476.190 | 1.395 |
| 4 | 0.072 | 180 | 555.556 | 1.628 |
| 4 | 0.072 | 170 | 588.235 | 1.723 |
| 4 | 0.072 | 180 | 555.556 | 1.628 |
| 4 | 0.072 | 180 | 555.556 | 1.628 |

## 4.5 Experimental Applications

### 4.5.1 Shock-Fluid Interaction

The shock tube was used to conduct experiments to analyze the shock-fluid interaction. To examine the effects of shock waves and pressure waves on fluids of different properties, two tests were performed using liquids with distinct viscosity and density; water and glycerin. The results indicated that the lower viscosity fluid (water) exhibited a greater response to the shock wave compared to the higher viscosity fluid (glycerin).
For the experimental setup, a plate was placed at the end of the driven section, parallel to the flow direction of the shock wave. Water and glycerin droplets were placed on the plate's hygroscopic surface to ensure direct interaction with the incoming shock wave. The plate itself did not obstruct the flow, allowing an unimpeded study of the fluid's response to the shock wave.
When the shock wave impinged on the fluid, the initial response was similar in both cases. The pressure wave induced a shear force on the shock-facing side of the droplet, causing it to be accelerated by the flow. The interaction resulted in a slight concave deformation on the rare surface of the droplet. Subsequently, the water drop was completely entrained by the incoming wave. However, in the case of glycerin, the droplet was not completely displaced; instead, a portion remained adhered to the surface, because of its higher viscosity and surface tension effects that resisted complete detachment.

(a) water (b) glycerine

Figure 4.16: fluid bubbles at t=0

(a) water (b) glycerine

Figure 4.17: Concave structure formed at rare side offluid drops

(a) water (b) glycerine

Figure 4.18: Spreading patterns of fluids due to shockwave

### 4.5.2 Shock Tunnel Tests

The shock tube was connected to a Mach 6 axis-symmetric C-D nozzle with a throat diameter of 11 mm connected to a dump tank. The dump tank was evacuated to near vacuum pressure, and schlieren visualization was performed by placing various test objects in the setup to observe the effects of flow.

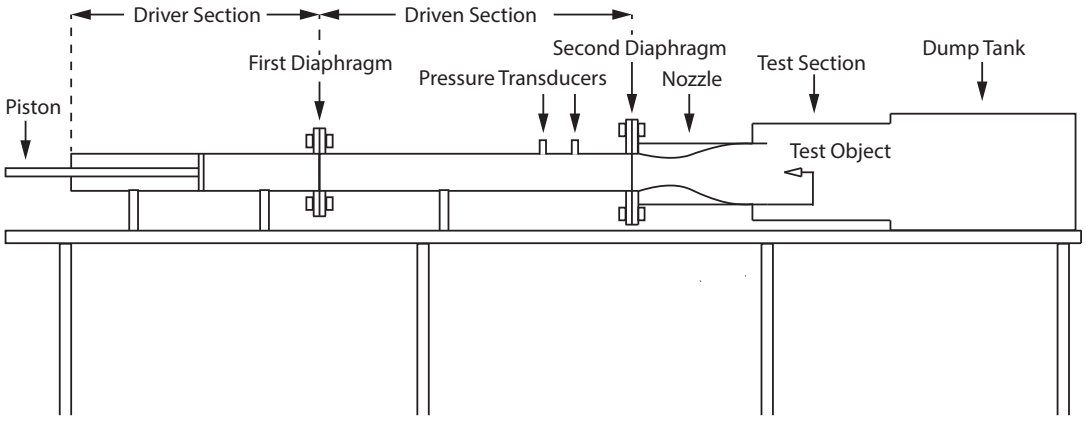


Figure 4.19: Shock Tunnel

The flow over a wedge and conical test object were visualized in the shock tunnel.

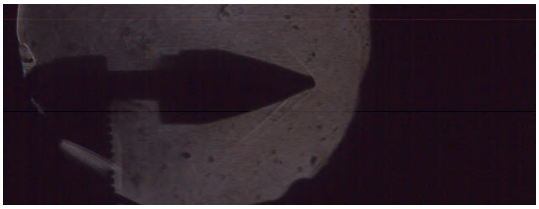

(a) Oblique shock-waves on $40^o$ conical test specimen

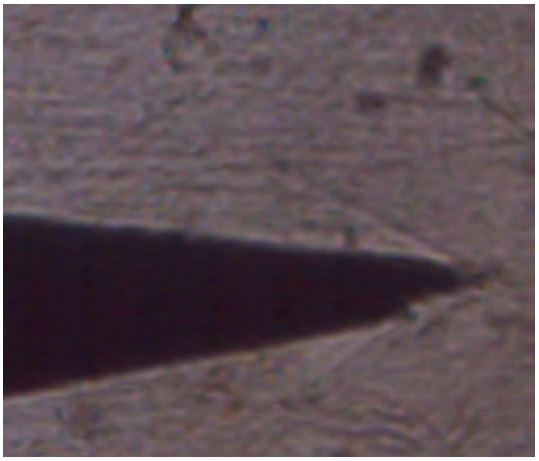

(b) Oblique shock-waves on $20^o$ wedge test specimen

Figure 4.20: Schlieren Images of Shock tunnel tests at M=5.5

## 4.6 Limitations

The limitations of the project are listed below:

- The intrusive pressure sensing setup might, to some extent, disturb the flow.
- The airgap between the layers of aluminum foil introduces uncertainty.
- The response time of transducer system is 10 $\mu s$ which limits the resolution of mach number measurement.

## 4.7 Problems Faced

The problems faced throughout the project were:

- Design of vacuum chamber for calibration of transducers was done from complete scratch and ensuring airtight wire connections was challenging.
- The Unavailability of electronic components was a challenge.
- Soldering of transducers in the small PCB designed was troublesome.
- Machining operations like honing during fabrication of SS tube were difficult.
- The debris from the diaphragm after bursting would fly with the flow and disturb flow visualization.
- The debris would usually stick to the nose of the transducers after getting burst, which would hinder pressure measurement.

## 4.8 Budget Analysis

Table 4.4: Budget Analysis

| S.N | Particulars | Amount (NRs) | Remarks |
|---|---|---|---|
| 1 | Shock Tube Fabrication | 25,000 | |
| 2 | NPP-301B-700AT transducer, amplifiers and pcb printing | 10,000 | |
| 3 | NI USB 6341 DAQ | - | Available in DMAE |
| 4 | Mounting components | 8,000 | |
| 5 | Documentation | 5,000 | |
| 6 | Miscellaneous | 10,000 | |
| | **Total** | **48,000** | |

The fabrication of the shock tube included material cost and machining cost. Mounting components include connectors, bolts, nuts, gaskets, washers, rubber seals, and pipe fittings. The project expenses covered documentation of the work, while minor expenses such as diaphragms, wires, and aluminum sections are considered under other miscellaneous costs. The necessary permissions were obtained from the relevant authorities to utilize the existing resources, including the DAQ system and single mirror Schlieren setup for the project.

## 4.9 Project Timeline

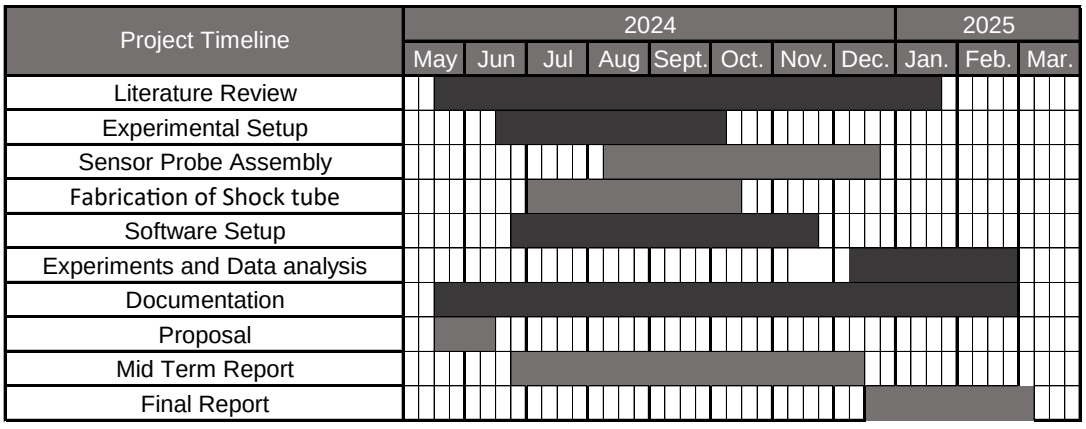


Figure 4.21: GANTT Chart

# CHAPTER FIVE:
# CONCLUSION AND SCOPE OF FURTHER ENHANCEMENT

## 5.1 Conclusion

The design and fabrication of the piston-driven supersonic shock tube was completed. The shock tube successfully generated supersonic flow, achieving a shock Mach number of up to 1.723 using a 0.072 mm aluminum diaphragm at a burst pressure ratio of 14.239. A high frequency pressure measurement system with sampling rate of 100 kS/s was made. The transducer was calibrated, the amplifier was tuned, and both were connected to the DAQ system for accurate data measurement. Velocity measurements, obtained through the ToF method with 100 mm transducer spacing, demonstrated consistent and repeatable results. This technique was used to calculate Mach numbers with varying diaphragm configurations. Using two, three, and four layers of 18 microns aluminum foil as a diaphragm resulted in maximum Mach numbers of 1.221, 1.395, 1.723 respectively. This indicates that as long as the tube can withstand the pressure and the required burst pressure is supplied, increasing the number of diaphragms leads to a higher Mach number. The resulting pressure waves were visualized using a single-mirror schlieren setup.

The burst pressure was characterized using *x/l* ratio. Using 2, 3, and 4 sandwiched layers of aluminum foil as diaphragms resulted in median burst pressure ratio of 4.96, 8.329, and 13.894, respectively. This research establishes a foundation for future experimental studies and characterization. Utilizing a shock tube, shock-fluid interactions in water and glycerin were examined, while shock waves were observed in various test specimens positioned within the test section of the shock tunnel. Schlieren imaging effectively captured shock wave propagation and external flow behavior, confirming the validity of the experimental setup and methodology.

## 5.2 Further Works

Further enhancements possible on the setup are:

- Fabrication of a probe for proper mounting of transducers.
- Implementation of fixed actuation system to enhance repeatability.
- Characterization of shock reflection pattern by placing pressure transducer at end wall of shock tube.

## REFERENCES


[1] I. Glass and G. Patterson, "A theoretical and experimental study of shock-tube flows," *Journal of the Aeronautical Sciences*, vol. 22, no. 2, pp. 73–100, 1955.

[2] J. D. Anderson, *Modern compressible flow: with historical perspective*, fourth edition ed. New York, NY: McGraw-Hill Education, 2021, oCLC: 1128891396.

[3] "piston motion in a free piston driver." [Online]. Available: https://shepherd.caltech.edu/T5/resources/FM88.pdf

[4] "diaphragm construction for free piston shock tube/tunnel." [Online]. Available: https://patentimages.storage.googleapis.com/0f/04/a5/e10241a12a3419/US5606110.pdf

[5] "Shock tube and shock tunnel : Design and experiments." [Online]. Available: https://apps.dtic.mil/sti/tr/pdf/ADA568015.pdf

[6] K. P. Lynch, S. M. Spitzer, T. W. Grasser, R. W. Spillers, P. A. Farias, and J. Wagner, "A free-piston driven shock tube for generating extreme aerodynamic environments: design and first shots." Sandia National Lab.(SNL-NM), Albuquerque, NM (United States), Tech. Rep., 2018.

[7] A. A. Zaidi, K. Mushtaq, and M. Asif, "Design and fabrication of supersonic shock tube capable of producing shock waves," 06 2017.

[8] T. Aro and D. Walsh, "Microwave interference method of measuring shock velocity in a shock tube," *Journal of Scientific Instruments*, vol. 43, no. 8, p. 572, 1966.

[9] M. DUNN, "Application of microwave and optical diagnostic techniques in shock-tube and shock-tunnel flows," in *3rd Aerodynamics Testing Conference*, 1968, p. 394.

[10] B. Medhi, G. M. Hegde, and K. J. Reddy, "Time-resolved quantitative visualization of complex flow field emitted from an open ended shock tube using a wavefront measuring camera," *Optics and Lasers in Engineering*, vol. 122, pp. 354–360, 2019.

[11] Y. Shi, D. Kong, X. Ma, and C. Zhang, "Dynamic calibration method of blast pressure pencil probes based on adjustable shock tube," *IEEE Sensors Journal*, vol. 23, no. 11, pp. 11 704–11 712, 2023.

[12] P. Gnemmi, J. Srulijes, and F. Seiler, "Overview of activities at the isl hypersonic shock tunnels," *International Journal of Engineering Systems Modelling and Simulation*, vol. 3, no. 1-2, pp. 74–86, 2011.

[13] "LABORATORY FOR HYPERSONIC AND SHOCK WAVE RESEARCH." [Online]. Available: https://aero.iisc.ac.in/people/lhsr/assets/documents/LHSR_brochure.pdf

[14] D. C. Berridge and S. P. Schneider, "Calibration of pcb-132 sensors in a shock tube," in *RTO AVT-200 RSM-030 Specialists"Meeting on Hypersonic Laminar-Turbulent Transition*, no. NF1676L-13491, 2012.

[15] R. Sriram, S. Ram, G. Hegde, M. Nayak, and G. Jagadeesh, "Shock tunnel measurements of surface pressures in shock induced separated flow field using mems sensor array," *Measurement Science and Technology*, vol. 26, no. 9, p. 095301, 2015.

[16] "A SHOCK TUBE FOR DOWNSELECTING MATERIAL CONCEPTS FOR BLAST PROTECTION PART I: DESCRIPTION OF THE SHOCK TUBE AND A COMPARISON OF FLUSH MOUNTED AND RECESS MOUNTED PRESSURE SENSORS ." [Online]. Available: https://apps.dtic.mil/sti/pdfs/ADA506204.pdf

[17] R. A. Segars and M. G. Carboni, "A shock tube for downselecting material concepts for blast protection, part i: Description of the shock tube and a comparison of flush mounted and recess mounted pressure sensors," *US Army Natick Soldier Research, Development and Engineering Center, Natick, MA, Technical Report*, no. 01760-5000, 2008.

[18] T. Singh and K. Reddy, "Test gas slug characterization for large-scale shock tube facility," *AIAA Journal*, vol. 55, no. 9, pp. 2912–2918, 2017.

[19] S. Murray, F. Zhang, K. Gerrard, P. Guillo, and R. Ripley, "Influence of diaphragm properties on shock wave transmission," in *Shock Waves: Proceedings of the 24th International Symposium on Shock Waves Beijing, China July 11–16, 2004*. Springer, 2005, pp. 801–806.

[20] S. Janardhanraj, S. Karthick, and A. Farooq, "A review of diaphragmless shock tubes for interdisciplinary applications," *Progress in Energy and Combustion Science*, vol. 93, p. 101042, 2022.

[21] H. A. Khawaja, J. Kapaya, and M. Moatamedi, *Shock Tube. Detail overview of equipment and instruments in the shock tube experimental setup*, 2015.

[22] "Product Documentation - NI-USB-6341 Specifications." [Online]. Available: https://www.ni.com/docs/en-US/bundle/usb-6341-specs/page/specs.html

[23] K. Thirumalesh, S. P. Raju, H. M. Somashekarappa, and K. Swaroop, "Shock tube data processing tools using open source hardware and software platforms," *Engineering Reports*, vol. 3, no. 9, p. e12353, 2021.

[24] A. Mazumdar, "Principles and techniques of schlieren imaging systems," 2013.

[25] G. S. Settles and M. J. Hargather, "A review of recent developments in schlieren and shadowgraph techniques," *Measurement Science and Technology*, vol. 28, no. 4, p. 042001, 2017.

[26] J. Meng and T. Colonius, "Numerical simulations of the early stages of high-speed droplet breakup," *Shock waves*, vol. 25, no. 4, pp. 399–414, 2015.

[27] A. Hanson, E. Domich, and H. Adams, "Shock tube investigation of the breakup of drops by air blasts," *Physics of Fluids*, vol. 6, no. 8, pp. 1070–1080, 1963.

[28] N. M. Reddy, "Development of a hypersonic shock tunnel," *Proceedings of the Indian Academy of Sciences. Section C, Engineering Sciences*, vol. 1, no. 1, pp. 73–92, 7 1978. [Online]. Available: https://doi.org/10.1007/bf02843516

[29] R. Bitter, T. Mohiuddin, and M. Nawrocki, *LabVIEW: Advanced programming techniques*. Crc Press, 2006.

[30] "Examining spatial (Grid) convergence." [Online]. Available: https://www.grc.nasa.gov/www/wind/valid/tutorial/spatconv.html

[31] E. M. Rothkopf and W. Low, "Diaphragm opening process in shock tubes," vol. 17, no. 6, pp. 1169–1173. [Online]. Available: https://pubs.aip.org/pfl/article/17/6/1169/894788/Diaphragm-opening-process-in-shock-tubes